INSTITUTE OF PHYSICS PUBLISHING JOURNAL OF OPTICS B: QUANTUM AND SEMICLASSICAL OPTICS

J. Opt. B: Quantum Semiclass. Opt. **3** (2001) R1–R28 www.iop.org/Journals/ob PII: S1464-4266(01)18846-4

PhD TUTORIAL

Dynamics of Bose–Einstein condensation in a gas with attractive interactions

C A Sackett[1] **and R G Hulet**

Physics Department and Rice Quantum Institute, Rice University, Houston, TX 77005, USA

Received 9 November 2000, in final form 14 February 2001

Abstract

The nature of Bose–Einstein condensation (BEC) in atomic vapours depends critically on the mean-field interaction of the atoms. When this interaction is attractive, the number of atoms in the condensate is limited. The interplay of this limit and the natural growth of the condensate during BEC leads to complicated dynamical behaviour. We develop a model for this behaviour based on the nonlinear Schrödinger equation and the quantum Boltzmann equation. The condensate occupation number is predicted to oscillate rapidly as the condensate alternately fills and collapses, and the oscillations are seen to persist for many cycles before the gas comes to equilibrium. Experimental evidence for these oscillations in the case of ^{7}Li is presented, along with details of the experimental apparatus and methods.

Keywords: Bose–Einstein condensation, ultracold atomic gas

1. Introduction

The development of techniques to produce Bose–Einstein condensation (BEC) in dilute atomic vapours has led to a surge of interest in condensate physics. This paper is intended to provide an introduction to the field. In particular, many of the properties of condensates arise from the effects of interatomic interactions. Atomic species with effectively attractive interactions are an especially good example of this, because in these gases condensates cannot exist if the interactions are too strong. This paper attempts to explain, in a self-contained way, why this is so and how the behaviour of condensates, when they do exist, is affected. Reference is generally made to the case of ^{7}Li, and to the experiments exploring its properties which we have carried out. The arguments and conclusions, however, are applicable to any species with attractive interactions.

The paper is divided into four sections. This first one provides a qualitative overview of BEC and the role atomic interactions play in the properties of a condensate. It is very much intended for the non-specialist, and we hope it will be of some value even to the non-physicist. The second section presents a brief but mostly self-contained development of the theoretical framework required to handle interacting atomic gases. The third section describes a numerical model we developed to simulate the gas, and explains the predicted behaviour. The fourth section discusses our experimental implementation and results.

1.1. What is BEC?

Bose–Einstein condensation is a phase transition that occurs when a collection of identical bosons is cooled to the point that their quantum mechanical de Broglie waves overlap. What exactly this means will be discussed at some length in the following, but the most important point is that BEC occurs only at quite low temperatures. The de Broglie wavelength Λ is equal to $\hbar/p$, where $\hbar$ is Planck's constant and p is the momentum of the particle. At temperature T, typical values of p will be $(2mk_{\mathrm{B}}T)^{1/2}$, where m is the mass of the particle and k_{B} is Boltzmann's constant. The precise condition for BEC to occur is that

$$n\Lambda^3 = n\left(\frac{2\pi\hbar^2}{mk_{\mathrm{B}}T}\right)^{3/2} = 2.612, \tag{1}$$

where n is the number density of the particles. The lower the density, the colder the required temperature is. BEC-like behaviour can occur in solid, liquid or gas phases, with observed transition temperatures ranging from a few degrees Kelvin for the densest systems to well below one millionth of a degree for the most dilute gases.

[1] Current address: Physics Department, University of Virginia, Charlottesville, VA 22904, USA.

BEC was predicted by Einstein in 1925 [1], in an extension to Bose's derivation of the Planck black-body radiation spectrum [2]. The theory of BEC was first applied to superfluid liquid helium in the 1930s and 40s [3,4], and shortly thereafter was used to explain superconductivity in metals at low temperatures [5]. These two branches of condensed matter physics have been enormously important research areas since their inception. More recently, BEC and related phenomena have been studied in several gaslike systems, such as excitons in a semiconductor crystal [6,7], liquid helium wetting a porous glass [8, 9] and spin-polarized atomic hydrogen on a liquid helium surface [10]. However, the experimental system closest to Einstein's original vision is probably the type described here, using a spin-polarized dilute atomic gas confined in a magnetic trap.

These experiments have been performed on a range of gases, namely ^{87}Rb, ^{7}Li, ^{23}Na, ^{1}H and ^{85}Rb [11–15, respectively]. Other species in which BEC is currently being pursued include the remaining alkali elements and metastable ^{4}He. A variety of phenomena have been investigated, such as excitation spectra [16, 17], coherence properties [18, 19], interference [20, 21] and multiple-spin-component gases [22, 23]. However, the field is still rapidly expanding, with many new experiments recently coming online or under development.

Atoms in these experiments are confined by magnetic fields in an ultra-high-vacuum chamber, so that they have no contact with their environment. This allows the gas to be kept very cold, while the remainder of the apparatus is at room temperature. In our experiment, the fields provide a nearly spherical harmonic potential, in which the ^{7}Li atoms oscillate with a frequency of $\omega \approx 2\pi \times 145$ Hz. The density of the gas is highest in the centre of the trap, and BEC occurs when this peak density satisfies (1). An equivalent formulation, in terms of the total number of trapped atoms N, is

$$N\left(\frac{\hbar\omega}{k_{\mathrm{B}}T}\right)^{3} = 1.202. \qquad (2)$$

We observe BEC to occur at a temperature of 700 nK, with roughly 1 million atoms in the trap. At this temperature, the gas forms a cloud about 0.1 mm in diameter. When BEC occurs, a significant number of atoms 'condense' into the quantum mechanical ground state of the trap. Spatially, this ground state consists of a narrow spike, about 6 μm in diameter, at the very centre of the cloud. The atoms in this state have many unusual properties.

Any standard textbook on statistical mechanics gives a derivation of (1), and a description of BEC in its simplest form [24, 25]. Fundamentally, understanding BEC means understanding such an approach, but it is also useful to try to develop a certain physical insight and intuition about the subject. Because BEC is an explicitly quantum mechanical phenomenon, it is outside the realm of direct human experience, and is difficult to explain in ordinary terms. However, many of its characteristics are shared with at least somewhat more familiar processes, and an understanding of it can to a degree be achieved through analogy with these processes. In combination with more precise mathematical descriptions, such analogies can be very fruitful.

For instance, BEC is a phase transition. That is to say, it is a process in which a macroscopic collection of particles changes physical state as its temperature is reduced. An apt example from daily life is the condensation of water from the air as dew. In the case of dew, the two phases are readily distinguished: water droplets are dense and almost incompressible, and have a well defined boundary separating them from the surrounding vapour. In general, a Bose condensate cannot be so easily identified. A better way to think of the change of state occurring in BEC is by analogy with the Curie transition in a magnetic material [26]. It well known that if a magnet is heated sufficiently, it will be demagnetized as the atomic magnetic moments composing it are randomized by thermal motion. As the material is gradually allowed to cool, the magnetization abruptly reappears at a critical temperature known as the Curie point. The transition is abrupt because, once a few neighbouring atoms find themselves aligned, they tend to force other nearby atoms to align as well, spreading the order rapidly through the material.

The Curie transition is easy to measure using a magnetometer, but lacking such a device it would be very difficult. It could be seen through subtle changes in the heat capacity of the material, or by direct probes of the atomic moments such as neutron scattering. Nonetheless, on the atomic level the transition marks a substantial change, as atoms from one side of the sample to the other all line up.

When BEC occurs in a gas, the atoms develop a uniform quantum mechanical phase in much the same way that atomic moments in a magnet develop a uniform orientation. Although this phase itself is fundamentally unobservable by direct means, it has a variety of effects which have been observed. The analogy is, then, that BEC bears a relation to a gas which is similar to the relation between the Curie transition and a solid. In both cases, a type of global order develops which is not necessarily apparent from an external viewpoint. The analogy serves well to illustrate the fallacy of considering a Bose condensate as a 'fourth phase of matter', after solids, liquids and gases. Just as a magnetized chunk of iron is still a solid, a Bose-condensed gas is still a gas.

The above analogy is of little help, however, in interpreting the meaning of a collection of atoms having an identical quantum phase. Fortunately, another more familiar example of a similar phenomenon exists, which is laser light [27]. According to the wave/particle duality principle of quantum mechanics, a beam of light must in some respects be considered as an electromagnetic wave propagating through space and in some respects as a stream of particles, termed photons. When considered as a wave, the notion that a laser has a definite phase is easy to comprehend: at a particular point in space, there is an oscillating electric field whose phase is well defined. (Note that 'phase' here is used with a different meaning than in 'phase transition'.) In ordinary incoherent light, such as that from an incandescent bulb, this phase is absent. Although an electric field is present in both cases, in the latter it is randomly fluctuating rather than smoothly oscillating in time, so a value for the phase cannot be defined.

The electric field of a beam of photons is very much analogous to the wavefunction of a beam of atoms, and physical intuition developed regarding the one can be fruitfully applied to the other. The fact that an electric field is ordinarily thought

of as a classically defined and measurable quantity reflects the fact that it ordinarily describes a macroscopic number of photons. It is then possible to measure its amplitude and phase to high precision without appreciably disturbing its overall state. Matter wavefunctions more typically describe the state of only a single particle, so that the familiar uncertainty restrictions apply and the wavefunction cannot be directly observed. This dichotomy does not necessarily hold, however, as in the case of incoherent light described above, where the electric field of each photon is different. (More precisely, the probability of finding two photons in the same field mode is small.) Similarly, the wavefunction of a Bose condensate describes a large number of atoms, allowing the 'atom field' to be defined and observed to an unusual degree of precision.

The analogy between a Bose condensate and an electric field does beg the question of what, exactly, an electric field is. Nonetheless, given some familiarity with how laser beams behave, the comparison is useful. It has been observed that a Bose condensate forms a standing wave when confined in a cavity such as an atom trap [28], that two condensates interfere both in space [20] and in time [21] when overlapped and that a condensate expanding from a small source behaves much like light diffracting from a small aperture [11]. Just as for an electric field in a laser, it is possible to define and in principle measure a definite phase relationship between the atom field at any two points of a condensate. This is the reason that the order parameter associated with BEC is often described as the quantum phase, though a more precise definition would be as the condensate wavefunction itself.

The production of laser light relies on the ease of creating photons from other forms of energy. In a typical laser, a gain medium consisting of molecules in an excited state is surrounded by an optical cavity. As the molecules relax to their ground state they emit photons, a fraction of which are reflected by the cavity mirrors back to the gain medium. The electric field of this reflected light induces other molecules to radiate their energy into the cavity as well, thus amplifying the reflected light. As this continues, the amplitude of radiation in the cavity mode builds up and lasing occurs.

BEC is a quite different process, even though the end results are closely related. Since transforming other forms of energy into matter is difficult, atoms cannot be simply emitted into a cavity mode, but must be transferred to it from elsewhere. Further, BEC is an explicitly thermodynamical process, and describes the equilibrium state of the gas. A laser is in an explicitly nonequilibrium state, and is only maintained by continually adding energy to the system through the replenishing of the gain medium. The analogy of a Bose condensate to a laser beam does not, therefore, help answer the question of why a Bose condensate forms.

Surprisingly, the analogy to the Curie transition also fails to address this issue. The Curie transition, like all phase transitions except BEC, occurs because of interactions between the constituent particles. In the case of a magnet, neighbouring atoms are coupled by electronic forces which, in the right circumstances, creates a tendency for them to align. BEC, in contrast, is predicted to occur even in a perfectly ideal gas, and has been observed in very nearly ideal gases.

The answer lies in quantum statistical mechanics. A Bose condensate forms for no other reason than that it is the most likely configuration of a sufficiently cold collection of bosonic atoms. The standard calculation is shown in many textbooks, but involves abstractions such as the calculation of the partition function and the choice of a particular ensemble. A simple example serves better to illuminate the underlying idea. Rather than considering atoms, which have an infinite number of quantum states available, a finite system can be used. In particular, imagine a set of N 'Bose coins', identical particles which can each be in either of two states, H or T, with equal probability. Consider the probability P_H that all of the coins are in state H. If the coins were classical, distinguishable objects, each possible state of the collection could be labelled by an enumeration of the states of each coin. There are 2^N distinct enumerations, so the probability of any particular configuration, such as '$H\,H\,H\,\ldots\,H$', would be 2^{-N}.

If the coins are identical bosons, however, then it is fundamentally impossible to determine whether a particular coin is in a particular state. The configurations 'coin 1 in H and coin 2 in T' cannot be counted as distinct from 'coin 1 in T and coin 2 in H'. In both cases all that can be said is that there is one coin in H and one in T, so that only one configuration can be counted. Each possible configuration of N coins can thus be labelled simply by the number of coins in state H. Since this occupation number can range from 0 to N, P_H is $1/(N+1)$. For large N, this is tremendously greater than 2^{-N}.

This example shows that, because of their symmetric nature, a group of identical bosons is more likely to be found all in the same state than a similar group of distinguishable particles. In order to demonstrate how this brings about an abrupt transition such as BEC, it is only necessary to allow the probability of observing state H to vary. In a physical system, this occurs because at a finite temperature T, the probability of finding an atom in a state with energy E decreases as $\exp(-E/k_{\mathrm{B}}T)$, a fundamental result of classical statistical mechanics [25]. So, if the probability of a single coin being in H is p, then p is related to the temperature of the real gas. Specifically, the temperature is proportional to $-\ln p$, so the case $p = 1$ can be associated with $T \to 0$ (assuming the state H has lower energy than the state T). If we allow p to vary in this way, the relative probability of observing k coins in H becomes $p^k(1-p)^{N-k}$, so that the probability of observing all N coins in H is

$$P_H = \frac{p^N}{\sum_k p^k(1-p)^{N-k}}. \tag{3}$$

The denominator is the normalizing sum of the relative probabilities of each possible configuration. Recognizing that the sum can be expressed as a geometric series allows P_H to be simplified to

$$P_H = \frac{p^N(2p-1)}{p^{N+1}-(1-p)^{N+1}}, \tag{4}$$

which in the limit of large N becomes

$$P_H = \begin{cases} p^{-1}(2p-1) & (p > 0.5) \\ 0 & (p < 0.5). \end{cases} \tag{5}$$

The function (4) is plotted in figure 1 for $N = 1000$. The discontinuity at $p = 0.5$ is analogous to the phase transition of

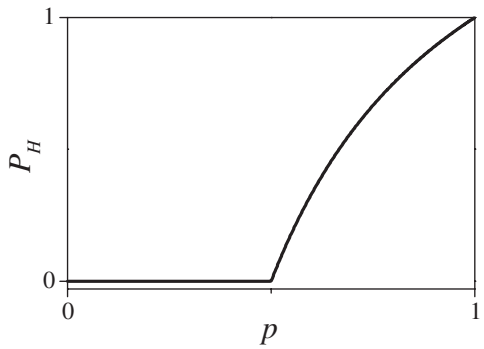

Figure 1. Phase transition in a set of quantum coins. The probability P_H that 1000 identical coins will be found all in state H is plotted versus the probability p that a single coin will be found in state H.

BEC, and arises for the same reason. The counting argument described is peculiar compared with the methods of normal statistics, but it is precisely that used in the standard derivation of BEC. It is instructive that it yields similar results even in so simple a system.

The three models discussed in this subsection cover, it is hoped, most of the more counterintuitive aspects of BEC. However, they are analogies only, and have their limits. Like the Curie transition, BEC is a phase transition marked by the development of a global order that does not necessarily correspond to a visible change in physical state. In the particular case of a magnetically confined gas, there in fact is an observable change of state, since the Bose condensate is localized in the centre of the trap. But the point of the comparison remains true, because the development of a coherent quantum phase is certainly the fundamental characteristic of BEC. The meaning of the quantum phase can be understood by analogy with a laser beam, but the phenomena are not the same. Atoms obey the Schrödinger equation, while photons obey Maxwell's equations; the detailed behaviour of the two systems will be different. Finally, although a set of quantum coins illustrates how the indistinguishability of quantum particles can lead to a phase transition, the transition obtained is not really BEC. For instance, the number of atoms in the lowest-energy state increases abruptly when BEC occurs, but when there are an infinite number of states available, the probability for all the atoms to be in the ground state remains negligibly small at any nonzero temperature.

1.2. Interactions

As mentioned above, BEC occurs even in an ideal gas of non-interacting pointlike particles. However, all real gases are composed of atoms which do interact. As the density of the gas is lowered, the importance of interactions is reduced as the atoms spend less and less time near each other. However, the interactions never vanish completely, and necessarily have a significant impact on BEC. Because of this significance, the different effects of interactions are discussed at some length here.

The vast majority of work on BEC has involved liquid helium or superconductivity, where interactions are complicated and have as important an effect on the behaviour of the system as have the quantum statistical effects. In contrast, the benefit of studying BEC in a dilute gas is that interactions cause only a small perturbation to ideal-gas behaviour. In particular, the density is low enough that there is a vanishingly small probability for three atoms to be near each other at the same time, so that three-body processes can usually be neglected compared to two-body binary interactions.

An obvious binary process is the elastic collision, where two atoms approach one another, interact as they pass and then fly apart on altered trajectories. The total kinetic energy of the two atoms is unchanged, but energy can be exchanged between them. It is this exchange of energy that allows the gas to come to thermal equilibrium, so that elastic collisions are directly responsible for the actual occurrence of BEC. In fact, consideration of these collisions alone provides a means of analysing the equilibrium state of the gas. This approach is explained here because it is relatively elementary but is not so familiar as the usual development.

Suppose that the number of atoms in a gas in state A is f_{A}, and define $R_{\mathrm{c}}(\mathrm{A}, \mathrm{B}; \mathrm{C}, \mathrm{D})$ to be the rate at which atoms in states A and B collide and change their states to C and D. Clearly, R_{c} must be proportional to f_{A} and f_{B}, since the rate at which a collision occurs is proportional to the number of atoms available to collide. Less clearly, R_{c} depends on f_{C} and f_{D}. This is a consequence of the indistinguishability of the atoms. If it were possible to label two atoms a_1 and a_2, then the rate at which a_1 and a_2 collided would be independent of the presence or absence in the gas of some other atom a_3 in the same state that a_1 happens to acquire. However, such labelling is impossible. One result is that R_{c} for a Bose gas is twice as large as for an otherwise identical gas of distinguishable particles, since it must include both collisions where the atom initially in state A ends up in state C and ones where it ends up in state D. In addition, if there were already atoms in state C, then it is impossible to determine, after the collision, which of those atoms was the one which collided. Since all possible ways of getting to the same final configuration contribute to the rate, R_{c} is proportional to the number of atoms in state C after the collision, which is $1 + f_{\mathrm{C}}$. An identical argument applies if atoms in state D were present, so it must be that $R_{\mathrm{c}}(\mathrm{A}, \mathrm{B}; \mathrm{C}, \mathrm{D}) \propto f_{\mathrm{A}} f_{\mathrm{B}}(1 + f_{\mathrm{C}})(1 + f_{\mathrm{D}})$.

In equilibrium, the population of each state is, by definition, constant. Normally, this occurs because the forward and backward rates for each possible collision become equal. Setting $R_{\mathrm{c}}(\mathrm{A}, \mathrm{B}; \mathrm{C}, \mathrm{D}) = R_{\mathrm{c}}(\mathrm{C}, \mathrm{D}; \mathrm{A}, \mathrm{B})$ yields a condition on the populations f:

$$f_{\mathrm{A}} f_{\mathrm{B}}(1 + f_{\mathrm{C}})(1 + f_{\mathrm{D}}) = f_{\mathrm{C}} f_{\mathrm{D}}(1 + f_{\mathrm{A}})(1 + f_{\mathrm{B}}). \quad (6)$$

It is another property of thermal equilibrium that any two states with the same energy will have the same populations. It is therefore possible to express f_{A} as $f(E_{\mathrm{A}}) = N(E_{\mathrm{A}})/g(E_{\mathrm{A}})$, where E_{A} is the energy of state A, $N(E)$ is the number of atoms in the gas with energy E, and $g(E)$ is the number of states with energy E. If $\mathcal{F}$ is then defined as $\mathcal{F}(E) = f(E)/[1 + f(E)]$, equation (6) simplifies to

$$\mathcal{F}(E_{\mathrm{A}})\mathcal{F}(E_{\mathrm{B}}) = \mathcal{F}(E_{\mathrm{C}})\mathcal{F}(E_{\mathrm{D}}). \quad (7)$$

A further constraint arises because the collisions are elastic, so that $E_{\mathrm{A}} + E_{\mathrm{B}} = E_{\mathrm{C}} + E_{\mathrm{D}}$. Since (7) holds for all energies, it is true when $E_{\mathrm{C}} = 0$, which yields

$$\mathcal{F}(E_{\mathrm{A}})\mathcal{F}(E_{\mathrm{B}}) = Z\mathcal{F}(E_{\mathrm{A}} + E_{\mathrm{B}}) \quad (8)$$

with $Z \equiv \mathcal{F}(0)$. The only function satisfying this relation is $\mathcal{F}(E) = Z\exp(-\beta E)$, with β arbitrary. Solving in turn for f yields

$$f(E) = \frac{1}{Z^{-1}\exp(\beta E) - 1}, \tag{9}$$

the usual Bose–Einstein distribution function if β^{-1} is identified with the temperature and Z with the fugacity. From f, all other equilibrium properties of the gas are readily determined. The power and simplicity of this argument illustrate the importance of elastic collisions. For further discussion of this subject, see section 3.1.

The actual rate for elastic collisions—the prefactor multiplying R_c—must be determined numerically from knowledge of the molecular potential $U(r)$, which specifies the interaction energy between two atoms separated by a distance r. The way this calculation is performed is discussed in section 2. The result is that, at low temperatures, all of the molecular physics can be expressed by a single number, the scattering length a. For ^{7}Li, a has the value -1.46 nm [29].

It is possible to understand why the scattering process can be characterized by a single parameter without working through the detailed calculation. As mentioned above, BEC occurs when the de Broglie wavelength of the atoms in a gas becomes comparable to the average interparticle spacing. If the system is to be considered a dilute gas, however, the interparticle spacing must be much larger than the range of $U(r)$. Otherwise, the particles would be interacting continuously, and the system would be better described as a liquid. It follows, then, that Λ must be much larger than the range of U. Typically, the molecular potential is effective across a distance of the order of 1 nm, and the de Broglie wavelength is 1000 times greater. This means that it is incorrect to think of the atoms bouncing off each other like marbles or billiard balls. Rather, the collisions should be considered as waves diffracting off very small obstacles. The obstacles are so small that they can be considered as pointlike, in that it is impossible for the scattered wave to carry away any details of their structure. This is entirely analogous to the inability of a microscope to resolve details much smaller than the wavelength of light. The scattered field therefore must consist of a spherical wave, which is characterized only by its (possibly complex) amplitude. This amplitude is the scattering length. The units of a can also be understood from this argument, since a spherical wave is expressed as

$$\frac{\mathrm{e}^{\mathrm{i}kr}}{r}, \tag{10}$$

which requires an amplitude with units of length to cancel the factor of r in the denominator.

The probability for a collision to occur is proportional to the intensity of the scattered wave, and thus to a^2. Indeed, the collisional cross section is given by $\sigma = 8\pi a^2$ for identical bosons. The cross section gives the 'effective size' of an atom, in the sense that if an atomic beam with a flux of F atoms per unit time per unit area is incident on a single target atom, the collision rate will be σF.

The previous discussion pointed out that an atom in an ultracold gas is in one sense very small, since another atom must be within a range of 1 nm or so in order to interact with it, but in another sense very large, since its wavefunction extends across 1 μm or more. As a consequence, in a Bose condensate, where the interparticle spacing is small compared to Λ, an atom finds itself in a sense interacting with many other atoms at once, but colliding only infrequently. This seemingly paradoxical result is, of course, an expression of the particle/wave duality fundamental to quantum mechanics discussed earlier.

One observable consequence of this situation arises because, when two atoms have overlapping wavefunctions, the molecular interaction shifts the energy of the pair. This occurs because the interaction energy is very large when two atoms are close, so that the average interaction energy can be appreciable even if the probability of the atoms being close to one another is small. The size of the energy shift is proportional to the scattering length, since the amplitude of the scattered wave is a measure of the effective strength of the interaction potential. The magnitude of the shift can be computed from this fact, using dimensionality arguments: if a pair of particles has an unperturbed energy E which is shifted by ΔE, then the dimensionless ratio $\Delta E/E$ must be proportional to a/Λ, since Λ is the only other physical length scale characterizing the particles. If there are many atoms within a distance Λ, then the total shift will be

$$\frac{\Delta E}{E} \sim n\Lambda^3\frac{a}{\Lambda}, \tag{11}$$

where n is the density of atoms. The unperturbed energy E is, however, related to Λ through $E \sim \hbar^2/m\Lambda^2$, so that the shift itself is approximately

$$\Delta E \sim \frac{\hbar^2}{m\Lambda^2}n\Lambda^3\frac{a}{\Lambda} = \frac{\hbar^2 na}{m}. \tag{12}$$

A precise derivation is provided in chapter 2, and yields $\Delta E = 4\pi\hbar^2 na/m$. This interaction energy is a mean-field effect, since it is the result of averaging over the possible locations of the atoms in the gas.

At the relatively low densities of a dilute gas, ΔE is small compared to the transition temperature for BEC:

$$\frac{k_B T_c}{\Delta E} = \frac{(2\pi\hbar^2/m)(n/2.6)^{2/3}}{(4\pi\hbar^2 an)/m} \approx \frac{1}{an^{1/3}}. \tag{13}$$

The condition that the gas be dilute is just that $na^3 \ll 1$, so $\Delta E \ll k_B T_c$. However, ΔE can easily be large compared to the unperturbed energy of the Bose condensate. If the condensate is confined to a volume of size ℓ^3, its energy will be $E_0 \approx \hbar^2/m\ell^2$. Therefore,

$$\frac{\Delta E}{E_0} \approx \frac{\hbar^2 an/m}{\hbar^2/m\ell^2} = na\ell^2 \approx N_0\frac{a}{\ell}, \tag{14}$$

where N_0 is the number of atoms in the condensate and in the last step the relation $n \approx N_0/\ell^3$ was used. The dilute-gas condition, expressed in terms of N_0, a and ℓ, can be written $N_0^{1/3}a/\ell \ll 1$. Applying this constraint to (14) shows that $\Delta E/E_0$ must be small compared to $N_0^{2/3}$. However, N_0 can be very large, so that $\Delta E/E_0$ can still be much larger than 1.

The scattering length a can have either sign. It is negative for ^{7}Li and ^{85}Rb, and positive for the other gases in which BEC has been observed. When $a < 0$, ΔE is also negative, meaning

that the interaction between atoms is effectively attractive. This presents a problem for large N_0, because the derivative of the condensate energy with respect to density will be negative. To understand the difficulty, suppose that the condensate would have size ℓ in the absence of interactions. Then in the presence of interactions, the condensate will be smaller as the gas attracts itself together. But when ℓ decreases, the density rises, making the interactions even stronger, which in turn further decreases ℓ. There is no end to the process: the condensate can always reduce its energy by decreasing ℓ and increasing n. Eventually, n reaches a^{-3}, and the condensate can no longer be considered a dilute gas. Rather than BEC, some other type of phase transition occurs, from a gas to a denser liquid or solid phase.

Because of this instability, it was long thought that BEC could not occur in a gas with $a < 0$ [30, 31]. However, the problem only arises when N_0 is so large that E_0 is negligible compared to ΔE. For smaller N_0, the condensate energy will be

$$E = E_0 + \Delta E \approx \frac{\hbar^2}{2m\ell^2} + \frac{4\pi\hbar^2 N_0 a}{m\ell^3}. \qquad (15)$$

Since E_0 increases as ℓ decreases, it provides a positive pressure offsetting the attractive interactions, as long as N_0 is small enough. The maximum possible N_0 value which can be supported is that at which the compressibility $\mathrm{d}^2E/\mathrm{d}\ell^2 = 0$. Roughly, this occurs at $N_0 = N_m \approx \ell/|a|$. A more precise calculation is discussed in section 2, and yields $N_m = 0.57\ell/|a|$ for atoms confined in a spherically symmetric harmonic trap [32].

In our experiments ℓ is approximately 3 μm, so $N_m \sim 1250$ atoms, substantially larger than 1. With this many atoms, the quantum phase of the wavefunction is certainly well defined and measurable, so the atoms do form a genuine condensate. Furthermore, N_m increases as ℓ increases, suggesting that having negative a is not a significant limitation. However, as ℓ increases, the maximum condensate density N_m/ℓ^3 decreases rapidly. In comparison, the critical density for the BEC transition depends only on temperature, so that the fractional density of the condensate vanishes for large ℓ. If the condensate is to be distinguished, its density must be appreciable compared to the density of uncondensed gas, so that in a large container, BEC can only be observed at vanishingly small temperatures when $a < 0$.

The third and last significant type of interaction is inelastic collisions, which lead to heating and a loss of atoms from the trap. Inelastic processes occur because the atoms are in a highly excited, metastable state which can decay and release energy. The atoms are excited in two different ways.

First, each individual atom is in an excited spin state. The energy of an atom with magnetic moment $\boldsymbol{m}$ in a magnetic field $\boldsymbol{B}$ is given by $-\boldsymbol{m}\cdot\boldsymbol{B}$. The lowest-energy state is, therefore, the one with $\boldsymbol{m}$ and $\boldsymbol{B}$ maximally aligned. The energy of this state will always decrease as the field strength increases, so an atom in this state will be attracted to a maximum in B. However, Maxwell's equations prohibit the existence of a maximum of B in free space, so a magnetic trap is ordinarily constructed by establishing a minimum in B, and trapping an atomic state with $\boldsymbol{m}$ antiparallel to $\boldsymbol{B}$. It is therefore possible for the spin, which determines $\boldsymbol{m}$, to relax to a lower-energy state.

In principle, an excited atom will eventually decay by spontaneously emitting a photon, but the rate for this to occur is very slow, on the order of once every 10 million years. Instead, relaxation usually occurs during a collision, where the internal energy can be transferred to the motion of the atoms. Linear momentum is conserved by splitting the energy evenly between the two atoms. However, since the spin state is changing, it is necessary to conserve angular momentum too. If the atomic moments are not already perfectly anti-aligned with $\boldsymbol{B}$, it is possible for one atom to flip and transfer its spin to the other; this is called spin exchange. This process happens relatively easily, but by storing the atoms with $\boldsymbol{m}$ and $\boldsymbol{B}$ perfectly anti-parallel, we suppress it. Since both atoms start out with the maximal amount of spin angular momentum, it is impossible to transfer any from one to the other.

The second way to conserve angular momentum is to transfer it from the spin of the atom to the orbital motion of the two atoms about their centre of mass. The spin and motional degrees of freedom are coupled by the interaction of the two magnetic dipole moments, so this process is termed dipolar relaxation. The dipole–dipole interaction is very weak, so collisions of this type occur only infrequently, but they are nonetheless the dominant loss mechanism in our experiment. They proceed at a rate proportional to the density, since the rate for a given atom to collide depends linearly on the number of other atoms available for it to collide with.

Just as each atom is individually in an excited state, the collection of atoms as a whole is only metastable. Lithium is a solid metal at room temperature, and certainly prefers to be a solid at the ultracold temperature at which our experiments are performed. In order for a solid to form, however, atoms must first bond to form molecules, molecules must join to form clusters, and clusters must come together to form a crystal. The initial stage of this recombination process cannot occur during a binary collision. If two atoms were to collide and stick together, the molecule formed would necessarily be at rest in the centre-of-mass frame. However, a tremendous amount of energy is released when the atoms bind, which then has nowhere to go. If the process is to occur, a third atom must be present in the collision to carry this excess energy away. Even then, the energy released is generally sufficient to allow all three atoms to escape the trap, so the thermodynamically favoured crystallization process can never get started. Ordinarily, the density of the gas is so low that three-body collisions are very uncommon, and this loss mechanism is not observed in our experiments. However, mean-field interactions cause the density to increase greatly when a condensate is unstable, and molecular recombination does occur in that circumstance.

A final loss mechanism is due, not to interactions between trapped atoms, but between trapped atoms and untrapped, room-temperature molecules in the vacuum chamber. Collisions with these background molecules knock atoms out of the trap at a steady rate. In our experiment, the vacuum pressure is low enough that this rate is small compared to that for dipolar relaxation.

1.3. Dynamics of BEC in ^{7}Li

The three types of interaction discussed above combine and lead to a surprising richness of behaviour in BEC. This paper will necessarily focus on the particular case of ^{7}Li, but other

systems are interesting as well. To give just one example, if two condensates of different species are created in the same trap and the mutual scattering length of the two species is positive, the condensates will repel one another [23,33]. When the densities are high enough, the condensates are immiscible, just like oil and water. As mentioned previously, however, the condensates are not liquids, but definitely gases. The possibility of oxygen and nitrogen in the air spontaneously separating is an alarming one, but the phenomenon occurs only because the condensates are, in a sense, strongly interacting gases. Such gases represent a new domain of physics, even aside from their phase-coherent properties as condensates.

When $a < 0$, the strongly interacting regime is unattainable, since N_0 is limited. What happens, though, if N_0 is gradually raised from below N_m to above it? This occurs naturally as the gas is cooled, since the condensate fraction grows as T is reduced. Clearly, at some point the condensate becomes unstable and begins to collapse upon itself. But how is this collapse initiated? How does it proceed? What remains in the trap when it is completed? It is these questions which are the subject of our investigations here. Although many details remain to be clarified, the general idea of this dynamics is now known.

When a ^{7}Li gas is cooled down to the critical temperature for BEC, the condensate forms and begins to grow. Atoms are transferred into the condensate through elastic collisions, but because the collision rate is finite and an atom must generally undergo several collisions before entering the condensate, the growth of the condensate lags the cooling by an appreciable amount. At first, the mean-field interactions in the condensate are negligible, and the condensate is essentially like that of an ideal gas. As N_0 rises, however, the attractive interactions start to draw the condensate together. In our trap, it shrinks from a ball initially about 6 μm in diameter to about 4 μm diameter before becoming unstable.

As N_0 approaches N_m, the stability of the condensate becomes more and more marginal. Because the gas is not at zero temperature, there is some thermal excitation of the condensate motion: it jiggles, ripples, and pulsates in the trap. At some point, this thermal motion causes the density to increase enough that the condensate begins to collapse. Even if the gas were at $T = 0$, the collapse would be initiated for $N_0 < N_m$ by quantum mechanical tunnelling of the condensate from the marginally stable state to a denser collapsing state.

Once initiated, the collapse proceeds quickly, in a time on the order of the oscillation period of the atoms in the trap. During the collapse, the density rises, and with it the rate for inelastic collisions. When the density becomes high enough for three-body recombination to be significant, the losses start to limit the density increase and the collapse begins to decelerate. It appears currently that the collapse halts with a few hundred atoms remaining in the condensate, which then re-expand. The atoms which are lost to inelastic collisions acquire a large amount of energy, and rapidly leave the trap. The process is thus reminiscent of a stellar nova, where a star first implodes under its gravitational attraction and then explodes, blowing off a fraction of its atmosphere and leaving a core behind.

In the case of the trapped atoms, however, a surrounding cloud of noncondensed gas remains. It is essentially unaffected by the collapse, since the noncondensed atoms have too much kinetic energy to be caught up in the collapse itself, and the ejected atoms most likely pass through the cloud without suffering further collisions. After the collapse is complete, then, the filling process continues just as before. This leads to a cycle of filling and collapse which continues until either the noncondensed cloud runs out of atoms, or the gas is allowed to come to equilibrium.

The following sections detail the experimental and theoretical efforts that have gone into developing the preceding story, and outline the questions that remain to be answered.

2. Theory of interacting condensates

In the limiting case of an ideal gas, a Bose condensate is a reasonably simple object. It consists of many atoms, each having the same wavefunction ψ_0. This wavefunction obeys the single-particle Schrödinger equation, so that its characteristics and dynamical response can be readily calculated using standard techniques. Any observable quantity can be expressed as an expectation value over ψ_0 and evaluated.

The behaviour of a real gas, however, will be affected by interactions between its constituent particles. Even when the gas is dilute and the interactions weak, they can have a profound influence. This is particularly the case for attractive interactions, which limit the occupation number of the condensate and effectively prevent BEC from occurring in a spatially homogeneous system.

This section develops the methods used to account for interactions, and to predict the dynamical behaviour of the condensate under their influence. The presence of noncondensed atoms is mostly ignored for the moment, but will be taken up again in section 3.

2.1. Scattering and the nonlinear Schrödinger equation

In a dilute gas, the basic building block describing interactions is the scattering event: two more or less independent atoms approach each other, interact strongly but briefly, and then depart. Any theory of many-particle interaction must start by correctly describing this two-body process. The description given here is very much *ad hoc*, but a comprehensive treatment can be found in [34] and a more basic one in, for example, [35].

In the centre-of-mass frame, a collision between two atoms which interact via a molecular potential $U(|\boldsymbol{r}_1 - \boldsymbol{r}_2|)$ is mathematically equivalent to the scattering of a single fictitious particle with reduced mass $\bar{m} = m/2$ by a fixed central potential $U(r)$. The wavefunction of the particle will satisfy the Schrödinger equation,

$$\left(-\frac{\hbar^2}{2\bar{m}}\nabla^2 + U(r)\right)\psi(\boldsymbol{r}) = E\psi(\boldsymbol{r}). \tag{16}$$

At large r, it takes the asymptotic form

$$\psi(\boldsymbol{r}) \underset{r\to\infty}{\longrightarrow} \mathrm{e}^{\mathrm{i}kz} + f(\theta,\varphi)\frac{\mathrm{e}^{\mathrm{i}kr}}{r}, \tag{17}$$

where the first term represents the incoming wave propagating along an arbitrary direction z, and the second term is a scattered wave expanding from the origin. The wavenumber k is given

by $k = (2\bar{m}E/\hbar^2)^{1/2}$. The function f is termed the scattering amplitude, and is to be determined in terms of U.

For a spherically symmetric potential, ψ can be expanded as a superposition of eigenfunctions of angular momentum, $Y_{lm}(\theta, \varphi)$. Since the boundary condition (17) has azimuthal symmetry, m will be zero and both ψ and f are independent of φ. If $\psi(\boldsymbol{r}) = r^{-1}u_l(r)Y_{l0}(\theta)$, the radial wavefunction u_l will satisfy

$$\left(\frac{\mathrm{d}^2}{\mathrm{d}r^2} + k^2 - \frac{l(l+1)}{r^2} - \frac{2\bar{m}}{\hbar^2}U(r)\right)u_l = 0. \tag{18}$$

At large distances, the two atoms interact via the van der Waals force, so U behaves as C_6/r^6 for $r \to \infty$. The potential term will therefore be negligible compared to the angular momentum barrier at large r, unless $l = 0$. However, in the low-energy limit $k \to 0$, the classical turning point of the motion will be at $r \sim l/k$ and the particle will be unable to penetrate to small r and sample the potential. The solution to (18) will therefore be independent of U, so no scattering can occur. For this reason, the only partial wave contributing to f as $k \to 0$ will be $l = 0$.

For fixed small k, U can be neglected when $r \gg (C_6/k^2)^{1/6}$. Typically this distance is on the order of 5 nm. At larger r, u will be a solution to the free wave equation, which can generally be expressed

$$u(r) \underset{r\to\infty}{\longrightarrow} A\sin(kr + \delta) \tag{19}$$

for arbitrary A and δ. The phase δ is determined by the behaviour of u at small r; one way to determine it is to numerically solve (18) for $u(r)$, and fit its asymptotic form to (19).

The total wavefunction ψ is therefore asymptotic to

$$\psi(r) \to \frac{A}{\sqrt{4\pi}}\frac{\sin(kr+\delta)}{r} \equiv A'\frac{\sin(kr+\delta)}{r}, \tag{20}$$

since $Y_{00} = 1/\sqrt{4\pi}$. The amplitude A' is determined by the boundary condition (17). The $l = 0$ projection of the incident plane wave $\mathrm{e}^{\mathrm{i}kz}$ is $\sin(kr)/kr$, so the boundary condition can be rewritten

$$\psi \to \frac{1}{2\mathrm{i}kr}[(1 + 2\mathrm{i}kf)\mathrm{e}^{\mathrm{i}kr} - \mathrm{e}^{-\mathrm{i}kr}], \tag{21}$$

while the asymptotic solution is

$$\psi \to \frac{A'}{2\mathrm{i}r}(\mathrm{e}^{\mathrm{i}\delta}\mathrm{e}^{\mathrm{i}kr} - \mathrm{e}^{-\mathrm{i}\delta}\mathrm{e}^{-\mathrm{i}kr}). \tag{22}$$

Equating the amplitudes of the incoming waves yields

$$A' = \frac{\mathrm{e}^{\mathrm{i}\delta}}{k}, \tag{23}$$

and then equating the amplitudes of the outgoing waves provides an expression for the scattering amplitude

$$f = \frac{\mathrm{e}^{\mathrm{i}\delta}}{k}\sin\delta. \tag{24}$$

To see how δ behaves as $k \to 0$, it is useful to divide the range of r into an internal part, where U is appreciable, and an external part, where U can be neglected. If the division point r_p is small compared to k^{-1}, then the form of the wavefunction in the internal part will not depend significantly on k. Therefore, the logarithmic derivative of the true radial wavefunction at the radius r_p,

$$\left.\frac{u'}{u}\right|_{r_\mathrm{p}} \equiv \gamma_\mathrm{p}^{-1}, \tag{25}$$

will be nearly independent of k. In the external part, ψ takes on its asymptotic form, given by (19). The two expressions and their derivatives must agree at r_p, so that

$$\gamma_\mathrm{p}^{-1} = \frac{k}{\tan(kr_\mathrm{p} + \delta)}. \tag{26}$$

Expanding the tangent function and solving for $\tan\delta$ yields

$$\tan\delta = \frac{k\gamma_\mathrm{p} - \tan kr_\mathrm{p}}{1 + k\gamma_\mathrm{p}\tan kr_\mathrm{p}}, \tag{27}$$

which in the limit of small k becomes

$$\tan\delta = k(\gamma_\mathrm{p} - r_\mathrm{p}). \tag{28}$$

The term on the right of (28) appears to depend on r_p, but δ itself is a genuine physical quantity independent of the arbitrary choice of division point. The dependence on r_p must therefore cancel, and δ must tend to zero like $-ka$ for some constant a. This constant is the s-wave scattering length, known to be -1.46 nm for ^{7}Li [29]. In the zero-energy limit, the scattering amplitude $f = -a$, so the scattering length completely characterizes an ultracold collision.

The scattering amplitude directly gives the partial cross section for scattering into angle θ, by

$$\frac{\mathrm{d}\sigma}{\mathrm{d}\Omega} = |f(\theta)|^2, \tag{29}$$

which can be derived by calculating the probability current

$$\boldsymbol{j} = \frac{\hbar}{2\bar{m}\mathrm{i}}(\psi^*\nabla\psi - \psi\nabla\psi^*) \tag{30}$$

for the scattered wavefunction (17). So, in the low-energy limit the total cross section is $\sigma = 4\pi a^2$. This result is modified for identical bosons, however, since scattering by an angle θ is indistinguishable from scattering by $\pi - \theta$. Both processes contribute coherently to the cross section, giving

$$\left.\frac{\mathrm{d}\sigma}{\mathrm{d}\Omega}\right|_\theta = \frac{1}{2}|f(\theta) + f(\pi - \theta)|^2. \tag{31}$$

The factor of $1/2$ reflects the fact that half the flux is scattered into an angle θ and half into $\pi - \theta$. The net result is to increase the s-wave cross section by a factor of 2, to $\sigma = 8\pi a^2$.

It will be useful to express a more directly in terms of the molecular potential $U(r)$. One way to accomplish this is by formally writing the scattered wavefunction as

$$\psi(\boldsymbol{r}) = \mathrm{e}^{\mathrm{i}kz} + \frac{2\bar{m}}{\hbar^2}\int \mathrm{d}^3r'\, G(\boldsymbol{r}, \boldsymbol{r}')U(\boldsymbol{r}')\psi(\boldsymbol{r}'). \tag{32}$$

The kernel G is the Green function for the free space Schrödinger equation, satisfying

$$(\nabla^2 + k^2)G(\boldsymbol{r}, \boldsymbol{r}') = \delta^3(\boldsymbol{r} - \boldsymbol{r}'). \tag{33}$$

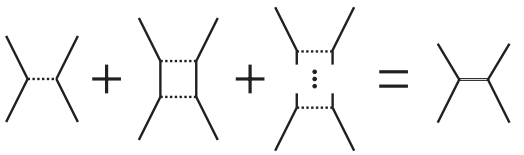

Figure 2. Summation of the ladder diagrams. The true molecular interaction between atoms is strong, and must be calculated to all orders in perturbation theory. This is equivalent to summing the series represented on the left. Knowing the sum, however, the interaction potential can be replaced with an effective potential which gives the correct result in first order, as represented on the right.

That (32) gives a solution to (16) can be verified by direct substitution. The Green function is

$$G(\boldsymbol{r},\boldsymbol{r}') = -\frac{\exp(\pm \mathrm{i}k|\boldsymbol{r}-\boldsymbol{r}'|)}{4\pi|\boldsymbol{r}-\boldsymbol{r}'|}, \tag{34}$$

where the + sign in the exponent must clearly be used if the boundary condition (17) is to be satisfied.

The asymptotic form of (32) is obtained by expanding G using $|\boldsymbol{r}-\boldsymbol{r}'| \to r - \hat{\boldsymbol{r}}\cdot\boldsymbol{r}'$, and yields

$$\psi \to \mathrm{e}^{\mathrm{i}kz} - \frac{\bar{m}}{2\pi\hbar^2}\frac{\mathrm{e}^{\mathrm{i}kr}}{r}\int \mathrm{d}^3r'\, \exp(-\mathrm{i}k\hat{\boldsymbol{r}}\cdot\boldsymbol{r}')U(\boldsymbol{r}')\psi(\boldsymbol{r}'). \tag{35}$$

The integral in (35) is denoted $T(\boldsymbol{k}_r,\boldsymbol{k}_z)$, and gives the amplitude for a particle originally travelling with momentum $\hbar k\hat{\boldsymbol{z}}$ to be found with momentum $\hbar k\hat{\boldsymbol{r}}$. Comparison with the results of the preceding section shows that

$$T(\boldsymbol{k}_r,\boldsymbol{k}_z) \xrightarrow[k\to 0]{} \frac{2\pi\hbar^2 a}{\bar{m}} = \frac{4\pi\hbar^2 a}{m}. \tag{36}$$

This low-energy limit will be denoted T^{2B}, reflecting the fact that it describes a two-body process.

A simple approximation suggested by the form of (32) is to replace ψ in T^{2B} by the incident wavefunction $\mathrm{e}^{\mathrm{i}kz}$. This is nothing but the Born approximation, and is valid when U is weak. However, the molecular potential is not weak, and the Born approximation is a poor one. It can be recovered, however, through the use of a renormalization-like procedure. If U is replaced by a new potential which yields the correct value for T^{2B} in the Born approximation, then first-order perturbation theory can be used with this modified potential, and will give results correct to all orders. In diagrammatic terms, this is equivalent to replacing an infinite sum of two-body 'ladder diagrams' with a single modified diagram, as suggested in figure 2.

Since the range of U is anyway very small compared to the wavelength k^{-1}, a suitable choice for a modified potential is simply

$$\bar{U}(\boldsymbol{r}) = T^{2B}\delta^3(\boldsymbol{r}). \tag{37}$$

This $\bar{U}$ is usually called the pseudo-potential, and has found many applications in physics. It is important to remember that it is only accurate when applied as a first-order perturbation. A true delta-function potential gives no scattering at all.

With an understanding of binary interactions in hand, the problem of an interacting condensate can now be considered [36–38]. The condensate is characterized by a many-body wavefunction $\Phi(\boldsymbol{r}_1,\boldsymbol{r}_2,\ldots,\boldsymbol{r}_{N_0})$, which is a solution of the full Schrödinger equation

$$\hat{H}\Phi = \sum_i \left\{-\frac{\hbar^2}{2m}\nabla_i^2 + V(\boldsymbol{r}_i) + \frac{1}{2}\sum_{j\neq i} U(|\boldsymbol{r}_i-\boldsymbol{r}_j|)\right\}\Phi = E\Phi. \tag{38}$$

The trapping potential V is included. Since Φ is to describe a condensate, it is expected to consist of a product of single-particle wavefunctions

$$\Phi_0(\boldsymbol{r}_1,\boldsymbol{r}_2,\ldots,\boldsymbol{r}_{N_0}) = \prod_i \psi(\boldsymbol{r}_i). \tag{39}$$

The correct function for ψ can be determined using the variational principle, since the best functional form will be the one which minimizes the energy $\langle\Phi_0|\hat{H}|\Phi_0\rangle$. However, if arbitrary variations in ψ are allowed, the energy will clearly be minimized by $\psi = 0$, which is unphysical. It is necessary to maintain the normalization of ψ, or equivalently, the expectation value of the number operator $\hat{N}$,

$$\langle\Phi_0|\hat{N}|\Phi_0\rangle \equiv \langle\Phi_0|\sum_i \mathbb{I}|\Phi_0\rangle = N_0\langle\psi|\psi\rangle^{N_0}, \tag{40}$$

where $\mathbb{I}$ is the identity operator. This can be achieved by using a Lagrange multiplier μ, and minimizing $\langle\Phi_0|\hat{H}-\mu\hat{N}|\Phi_0\rangle$. Here μ plays precisely the usual role of the chemical potential; it will subsequently be seen that μ in fact is the chemical potential.

Evaluating the expectation value to be minimized yields

$$\begin{aligned}\langle\hat{H}-\mu\hat{N}\rangle &= \sum_i \int \mathrm{d}^3r_i \left\{\psi_i^*(H_i-\mu)\psi_i \right.\\ &\quad \left. +\tfrac{1}{2}\sum_{j\neq i}\int \mathrm{d}^3r_j\, \psi_j^*\psi_i^* U_{ij}\psi_i\psi_j\right\}\\ &= N_0\int \mathrm{d}^3r\left\{\psi^*(H_0-\mu)\psi + \frac{N_0-1}{2}\right.\\ &\quad \left.\times\int \mathrm{d}^3r'\,\psi'^*\psi^* U(|\boldsymbol{r}-\boldsymbol{r}'|)\psi\psi'\right\},\end{aligned} \tag{41}$$

with a subscript or prime indicating the argument of a function and

$$H_i = -\frac{\hbar^2}{2m}\nabla_i^2 + V(\boldsymbol{r}_i), \qquad H_0 = -\frac{\hbar^2}{2m}\nabla^2 + V(\boldsymbol{r}). \tag{42}$$

The interaction term will only be important when the occupation number of the condensate is large, so its coefficient can be safely simplified to $N_0/2$. Minimization is carried out using the variational calculus in the standard way, and results in

$$\begin{aligned}\delta\langle\hat{H}-\mu\hat{N}\rangle &= N_0\int \mathrm{d}^3r\left\{\delta\psi^*(H_0-\mu)\psi + \delta\psi(H_0-\mu)\psi^*\right.\\ &\quad \left. +N_0\int \mathrm{d}^3r'\,U(|\boldsymbol{r}-\boldsymbol{r}'|)\psi'^*\psi'[\psi\delta\psi^* + \psi^*\delta\psi]\right\}.\end{aligned} \tag{43}$$

Integration by parts was used to rewrite the $\psi^*\delta\nabla^2\psi$ term, and the dummy integration variables were interchanged on the two terms of the form $\psi\delta\psi'$. Since the real and imaginary parts of ψ can be varied independently, the coefficients in the integrand of $\delta\psi$ and $\delta\psi^*$ must independently vanish, implying that

$$\left\{H_0 - \mu + N_0\int \mathrm{d}^3r'\,U(|\boldsymbol{r}-\boldsymbol{r}'|)\psi'^*\psi'\right\}\psi = 0, \tag{44}$$

which is not quite right.

The problem with equation (44) is that the integral over U is huge, and diverges for the physically plausible case of particles with perfectly hard repulsive cores. What this points to is a failure of the original trial wavefunction Φ_0; in reality, the condensate wavefunction is not just a product of single-particle wavefunctions, but has a many-body correction part which is important whenever $|\boldsymbol{r}_i - \boldsymbol{r}_j|$ is small for some i and j. Since the range of U is very small, however, the product-state approximation should be adequate almost everywhere, and all that is needed is to know the effect of the many-body part on the interaction energy. Fortunately, this effect can be included nonperturbatively using the pseudo-potential approach described above. It is simply necessary to replace U in (44) with $\bar{U} \equiv T^{2B}\delta^3(\boldsymbol{r} - \boldsymbol{r}')$. The result is the nonlinear Schrödinger equation (NLSE) [37, 38],

$$-\frac{\hbar^2}{2m}\nabla^2\psi + V(\boldsymbol{r})\psi + N_0 T^{2B}|\psi|^2\psi = \mu\psi, \qquad (45)$$

which governs the behaviour of an interacting condensate. Equation (45) shows that μ is indeed the energy of a single atom in the presence of an existing condensate, which defines the chemical potential $\mu \equiv \partial E/\partial N$ [25].

In the case of ^{7}Li, a and thus T^{2B} is negative, indicating that the interaction energy of the condensate is negative. In section 1, it was concluded from this that the condensate occupation number must be limited, and this conclusion is born out by numerical solution of (45) [32, 39, 40]. If a spherically symmetric harmonic potential $V(\boldsymbol{r}) = m\omega^2 r^2/2$ is used, it is found that solutions exist only when N_0 is smaller than a critical value $N_m = 0.57\ell_0/|a|$, where $\ell_0 = (\hbar/m\omega)^{1/2}$ is the length scale of the condensate.

It will also be useful to express the total energy of the condensate as a functional of ψ, or

$$E[\psi] = \langle\Phi_0|H|\Phi_0\rangle = N_0\int \mathrm{d}^3r\,\psi^* \times\left[-\frac{\hbar^2}{2m}\nabla^2 + V(\boldsymbol{r}) + \frac{N_0}{2}T^{2B}|\psi|^2\right]\psi. \qquad (46)$$

The pseudo-potential has again been used to express the interaction term. Note that the total energy of the condensate is not the sum of the energies of the single-particle states. Rather,

$$E[\psi] = N_0\mu - \tfrac{1}{2}N_0 T^{2B}\int \mathrm{d}^3r\,|\psi|^4. \qquad (47)$$

This reflects the fact that the many-body part of the condensate wavefunction makes a significant contribution to the interaction energy.

The above discussion considered a time-independent situation, but the dynamical equation governing the condensate can be obtained with some additional effort [37]. As might be expected from (45), the time-dependent single-particle wavefunction $\Psi(\boldsymbol{r}, t)$ obeys

$$\mathrm{i}\hbar\frac{\mathrm{d}\Psi}{\mathrm{d}t} = \left(-\frac{\hbar^2}{2m}\nabla^2 + V + T^{2B}|\Psi|^2\right)\Psi \qquad (48)$$

with the separable solution $\Psi = \psi(\boldsymbol{r})\exp(-\mathrm{i}\mu t)$.

2.2. Variational approximation

The NLSE cannot be solved analytically, and even numerical solution is difficult when the interaction term is significant and negative, as will be discussed below. It is therefore sensible to attempt approximate solutions, in order to obtain some physical insight and a qualitative understanding of the condensate behaviour. One approach described here is based on a variational solution for ψ. In the absence of interactions, the NLSE reduces to the normal Schrödinger equation, and for a harmonic potential the solution for the ground state is a Gaussian function. Furthermore, because of the stability limit $N_0 < N_m$, the interaction term can never come to dominate the equation. A reasonable choice for a trial solution, then, is a Gaussian function with variable width. Wavefunctions of this form have been studied ever since it was first realized that solutions to the NLSE existed for $a < 0$ [41–43]. However, Stoof [43] has provided the most careful and complete development, and his approach is mainly followed here.

The true ground-state wavefunction ψ will minimize the condensate energy. If $V(\boldsymbol{r}) = m\omega^2 r^2/2$ is used in (46), then the trial wavefunction

$$\psi = \left(\frac{N_0}{\pi^{3/2}\ell^3}\right)^{1/2}\exp\left(-\frac{r^2}{2\ell^2}\right) \qquad (49)$$

gives an energy

$$E(\ell) = \frac{3\hbar^2 N_0}{4m}\left[\frac{1}{\ell^2} + \frac{\ell^2}{\ell_0^4} - \frac{4}{3\sqrt{2\pi}}\frac{N_0|a|}{\ell^3}\right], \qquad (50)$$

with $\ell_0 = (\hbar/m\omega)^{1/2}$. Expressed in terms of the dimensionless variable $q = \ell/\ell_0$, the energy simplifies to

$$E(q) = \frac{3N_0\hbar\omega}{4}\left(\frac{1}{q^2} + q^2 - \frac{\beta}{q^3}\right), \qquad (51)$$

where

$$\beta = \frac{4}{3\sqrt{2\pi}}\frac{N_0|a|}{\ell_0} \qquad (52)$$

characterizes the strength of the interactions.

The energy E is plotted in figure 3 for several values of β. A local minimum near $q = 1$ is observed when β is small, but the absolute minimum always occurs at $q = 0$. This quantitatively confirms the argument expressed in section 1.2. Note that, in reality, the energy will diverge to positive infinity as $q \to 0$, since the true molecular potential U has a steep inner wall arising from exchange effects. However, long before q is this small, the density will become comparable to $|a|^{-3}$ and the treatment of the condensate as a weakly interacting gas will fail. The graphs in figure 3 can only be taken to extend down to $q \gg |a|/\ell_0 \approx 5 \times 10^{-4}$ for the ^{7}Li parameters. This is, however, quite far into the unstable region, so that many details of a collapsing gas can be described by the NLSE.

If a local minimum at large q exists, it represents a metastable state for the condensate. The maximum value of β at which such a state is found is determined by solving simultaneously

$$\frac{\mathrm{d}E}{\mathrm{d}q} = \frac{\mathrm{d}^2E}{\mathrm{d}q^2} = 0, \qquad (53)$$

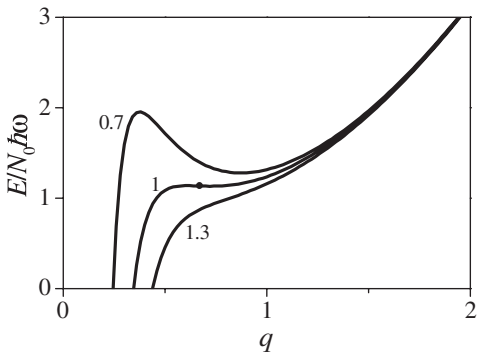

Figure 3. Variational calculation of condensate energy, using a Gaussian trial wavefunction. The energy E of a condensate with Gaussian radius ℓ is shown as a function of $q = \ell/\ell_0$. The strength of the interaction is parametrized by $\beta = 0.53N_0|a|/\ell_0$, with $\beta = \beta_c = 0.36$ at the stability limit. Each curve is labelled with its value of β/β_c.

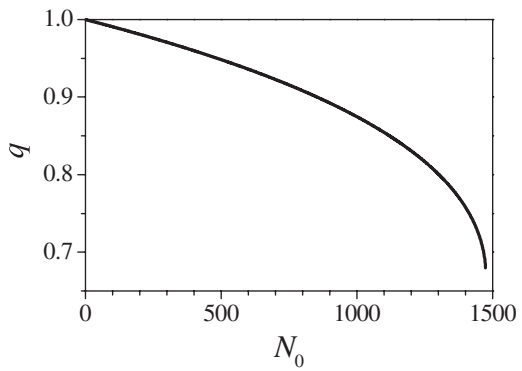

Figure 4. Condensate size in the variational approximation.

which occurs at the inflection point marked with a dot in figure 3. The values thus obtained are

$$q_c = 5^{-1/4} \tag{54}$$

and

$$\beta_c = \tfrac{8}{3}5^{-1/4}. \tag{55}$$

From β_c, the predicted value of N_m is found to be $0.67\ell_0/|a|$, about 20% greater than the valued obtained numerically from the NLSE. This comparison gives a measure of the accuracy of the Gaussian wavefunction approximation. For $N_0 < N_m$, the solution of $\mathrm{d}E/\mathrm{d}q = 0$ gives the size of the metastable condensate. Just before the collapse occurs, q shrinks to 0.67, indicating a density increase of a factor of 3.3. The dependence of q on N_0 is shown in figure 4.

The true utility of the variational approach comes from its application to dynamics. It is possible to show that the motion of the condensate can be treated as the motion of a quasiparticle with coordinate ℓ and mass m^*, moving on the potential surface $E(\ell)$ [43]. This provides a simple physical picture for the collapse process, where the quasiparticle is initially trapped in the local minimum at $q \sim 1$, but when N_0 is increased and the barrier falls, the condensate slides towards $\ell = 0$, like a marble rolling down a hill.

One dynamical quantity easily calculated in this framework is the frequency of the 'breathing mode' oscillation

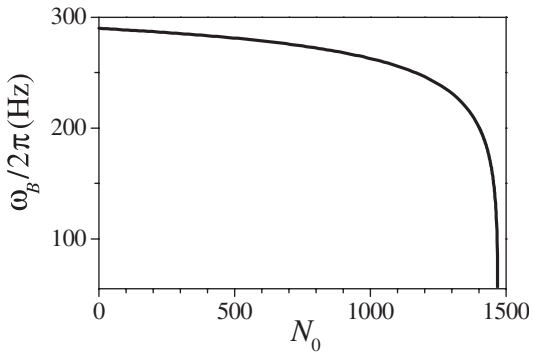

Figure 5. Breathing mode oscillation frequency ω_B for ^{7}Li in a symmetric trap with $\omega = 145$ Hz. The frequency approaches zero as the condensate becomes unstable with respect to compression.

of the condensate, which is determined by the curvature of E at the metastable minimum. The curvature cannot be expressed analytically, but is readily determined numerically by solving

$$\frac{\mathrm{d}E}{\mathrm{d}\ell} \propto q - q^5 - \frac{3}{2}\beta = 0 \tag{56}$$

for q_β and using this value in

$$\frac{\mathrm{d}^2E}{\mathrm{d}\ell^2} = \frac{3N_0\hbar\omega}{2\ell_0^2}\left(\frac{3}{q^4} + 1 - \frac{6\beta}{q^5}\right) \to \frac{3}{2}N_0m\omega^2\left(5 - \frac{1}{q_\beta^4}\right). \tag{57}$$

The breathing-mode frequency ω_B is then obtained from

$$\frac{1}{2}m^*\omega_\mathrm{B}^2\ell_0^2(q - q_\beta)^2 = \frac{1}{2}\frac{\mathrm{d}^2E}{\mathrm{d}\ell^2}\ell_0^2(q - q_\beta)^2, \tag{58}$$

or

$$\omega_\mathrm{B} = \omega\sqrt{\frac{3N_0m}{2m^*}(5 - q_\beta^{-4})}. \tag{59}$$

The effective mass m^* can be determined by ensuring that ω_B takes the correct value in the limit of a noninteracting gas $q_\beta \to 1$. Since each atom makes one half of a trap oscillation in one breathing mode oscillation, $\omega_\mathrm{B} \to 2\omega$ and $m^* = 3N_0m/2$. Thus ω_B is simply

$$\omega_\mathrm{B} = \omega\sqrt{5 - q_\beta^{-4}}, \tag{60}$$

which correctly approaches zero as $q_\beta \to q_c$. The dependence of ω_B on N_0 is shown in figure 5; a more complete treatment can be found in [44].

The dynamical picture can also be used to understand the initiation of a collapse. If N_0 is close to N_m so that a barrier is present but sufficiently small, the condensate will be able to tunnel through it. Using a semi-classical approximation for the tunnelling rate yields [43]

$$\gamma_0 = \sqrt{\frac{m^*\omega_\mathrm{B}v_B^2}{\pi\hbar}}\exp\left\{-\frac{1}{\hbar}\int_{\ell_1}^{\ell_2}\mathrm{d}\ell\,\sqrt{2m^*[E(\ell) - E(\ell_1)]}\right\}, \tag{61}$$

where ℓ_1 is the location of the metastable minimum, ℓ_2 the location on the inner side of the barrier where $E = E(\ell_1)$, and v_B is a parameter characterizing the barrier, which is on the order of ω_B times the peak width. The rate is plotted as

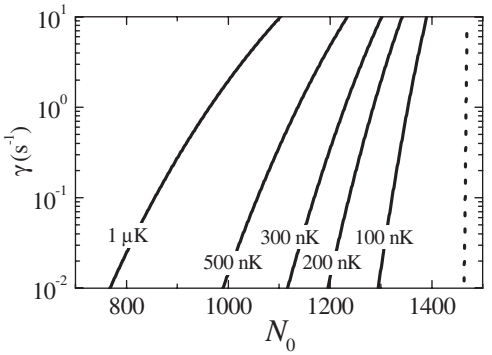

Figure 6. Collapse initiation rates γ as a function of condensate occupation number, for ^{7}Li in a symmetric trap with $\omega = 145$ Hz. The solid curves give the rates for thermal fluctuations at the temperatures shown, and the dashed curve gives the quantum tunnelling rate.

the dashed curve in figure 6. Note that the tunnelling process is a coherent one involving all N_0 atoms in the condensate. This is one of very few situations in physics where a relatively large composite object is predicted to exhibit tunnelling, and observation of the phenomenon would be a truly remarkable demonstration of quantum mechanics. Additional discussions of the tunnelling rate are given in [42, 45, 46].

For a condensate in a finite-temperature gas, however, the tunnelling effect is masked by the possibility for the collapse to be initiated by thermal fluctuations. In equilibrium, the breathing mode will be thermally excited, which can drive the condensate over the barrier when the barrier height becomes comparable to $k_B T$. The rate for this to occur is approximately

$$\gamma_T = \frac{\omega_B}{2\pi} \exp\left\{-\frac{E(\ell_m) - E(\ell_1)}{k_B T}\right\}, \tag{62}$$

where ℓ_m is the position of the barrier peak. The rate is plotted for several temperatures in figure 6. As can be seen, the thermal excitation rate dominates even for quite low temperatures; in order for tunnelling to be observed, an essentially pure condensate is required.

Finally, the Gaussian approximation can be used to investigate the dynamics of the collapse itself. Treated semi-classically, the condensate in the unstable regime will obey Newton's equations

$$m^* \ddot{\ell} = -\frac{dE}{d\ell}, \tag{63}$$

which can be solved numerically. However, during the collapse, atoms are lost due to inelastic collisions, and these losses must be accounted for by allowing N_0 to vary in time. Atoms are lost by two mechanisms, dipolar relaxation and molecular recombination. Dipolar relaxation is a two-body process which scales as the density n^2, while molecular recombination is a three-body process scaling as n^3. The loss rate from the condensate is therefore

$$\dot{N}_0 = -\int d^3r \left[\frac{2G_2}{2} n(\boldsymbol{r})^2 - \frac{3G_3}{6} n(\boldsymbol{r})^3\right], \tag{64}$$

which evaluates to

$$\dot{N}_0 = -\frac{N_0^2}{\pi^{3/2}\ell^3}\left(\frac{G_2}{2\sqrt{2}} + \frac{N_0 G_3}{6\sqrt{3}\pi^{3/2}\ell^3}\right) \tag{65}$$

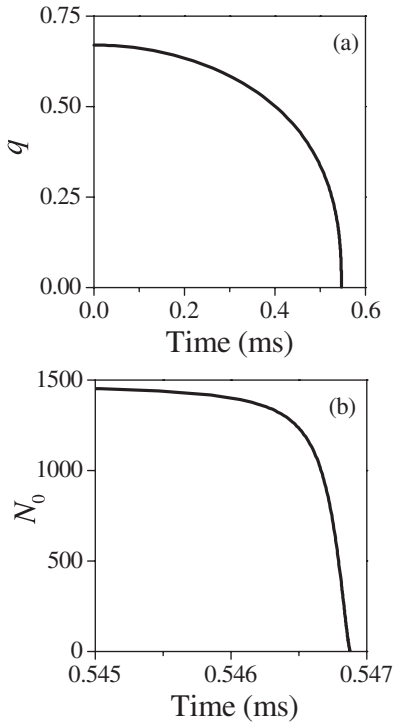

Figure 7. Collapse dynamics from the Gaussian approximation. (*a*) The evolution of condensate size q in time. (*b*) The evolution of occupation number N_0. The condensate was initially taken to have $N_0 = 1480$ and $q = 0.67$.

for a Gaussian density distribution. The G_i are the rate constants for the inelastic collisions. The coefficients in (64) reflect the definition of G_n as the rate coefficient for collisions in a nondegenerate gas. In each n-body collision, n atoms are lost, which provides the numerators. The denominators arise from the coherence properties of a condensate, which reduce the rate for n-body collisions by $n!$ [18]. The two coupled equations for q and N_0 can be solved together using standard techniques. The results are shown in figure 7. It is seen that the entire collapse occurs in less than a millisecond, and that virtually all of the atoms are lost.

2.3. Numerical solution of the NLSE

The variational method described above is a powerful technique which provides both physical insight and reasonably accurate quantitative results, at least in the stable regime. Although it makes predictions for the collapse dynamics, as in figure 7, it is possible that the assumption of a Gaussian wavefunction becomes inaccurate as the interaction energy becomes dominant. It is therefore desirable to compare the variational predictions with numerical solutions of the NLSE.

Numerical studies of the NLSE have a substantial history, since the same equation governs several classical nonlinear wave phenomena, notably in the propagation of deep-water waves [47], the collapse of Langmuir waves in plasmas [48], and the self-focusing of light waves in nonlinear media [49]. Zhakharov, in particular, has devoted much effort to the subject [50]. Accurate modelling of the collapse is known to be difficult, because of the large dynamic range in time and length scales required. In addition, the numerical simulation

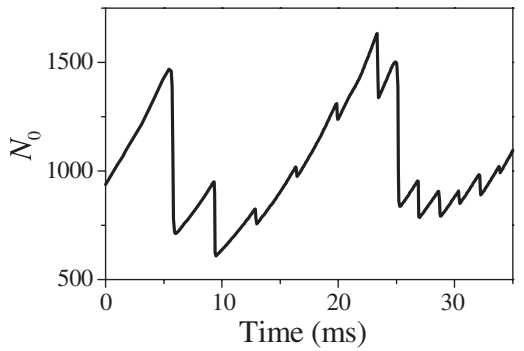

Figure 8. Numerical solution of the NLSE using the parameters of Kagan *et al* [51].

of trapped condensates involves several novel issues as to the growth and loss mechanisms at work.

The most straightforward way to include losses and growth in the NLSE is to add inelastic terms to the right-hand side of (48),

$$-\mathrm{i}\left(G_2|\psi|^2+\frac{G_3}{2}|\psi|^4\right)\psi+\mathrm{i}\xi\psi, \tag{66}$$

as in (64), also assuming a constant filling rate ξ. While this heuristic approach is unlikely to be exactly correct, Kagan *et al* [51] have used (66) to investigate the details of the collapse process. They report two main results. First, when a collapse occurs, roughly half the atoms in the condensate are lost. An example of the time dependence of N_0 is shown in figure 8. This is in contrast to the variational model, which predicts nearly all the atoms to be lost. Second, after the collapse, the condensate remaining is in a excited state. This excitation comes about because, after the collapse is halted, the atoms which were caught up in the collapse but not lost find themselves localized in a very small volume, and thus have a great deal of kinetic energy. As this excitation evolves, the condensate wavefunction becomes substantially different from a Gaussian, which calls into question the approximations of the variational approach.

Unfortunately, the parameters used by Kagan *et al* in their study did not correspond well to the experimental parameters of interest, so direct comparison with experimental results is difficult. The results do, however, point out that many aspects of the collapse process and condensate dynamics are not well understood, and suggest a rich and complex behaviour rewarding of further study. It is also to be hoped that experimental efforts will help shed light on these issues, a question which will be taken up again in section 4.

3. Kinetics of BEC

The previous section dealt with the properties of a Bose condensate, but if a condensate is to be studied, it must first be formed. Two processes are involved in this formation. First is the essentially experimental issue of creating a gas which is cold and dense enough for BEC to occur. One of the techniques used is evaporative cooling, in which the most energetic atoms in a thermal distribution are systematically removed. As the gas re-equilibrates, it cools. Evaporative cooling reduces the gas temperature by a factor of a thousand; it is a crucial stage of experiments without which BEC would not yet have been observed in a dilute gas. The second process is the action of condensation itself, in which elastic collisions deposit atoms into the ground state of the trap once the gas is cold enough. It is important to understand the rate at which this occurs, so that experiments can be performed on a suitable timescale. Furthermore, when $a<0$, the filling process affects the condensate behaviour directly, and must be understood if the dynamics of the collapse are to be accurately modelled.

Both of these issues relate to the redistribution of atomic energies through elastic collisions, properly the study of gas kinetics. In this section, kinetic theory is briefly developed and our implementation described. The model is then applied first to the problem of evaporative cooling [52], and then to the behaviour of a quantum degenerate gas [53].

3.1. The quantum Boltzmann equation (QBE)

The goal of kinetic theory is to understand the behaviour of the distribution of atoms in a gas. In classical mechanics, this distribution is characterized by the function $f(\boldsymbol{r},\boldsymbol{p})$, where

$$\mathrm{d}N=\frac{\mathrm{d}^3r\,\mathrm{d}^3p}{(2\pi\hbar)^3}f(\boldsymbol{r},\boldsymbol{p}) \tag{67}$$

is the number of particles in the volume d^3r at position $\boldsymbol{r}$ having momentum $\boldsymbol{p}$ in a range d^3p. For a quantum gas, this definition is inadequate since an atom does not have a well defined position or momentum. The analogue of f is then the Wigner function, which is an expression of the density matrix in a mixed position–momentum basis [54]. For a thermal gas, however, the quantum effects are small and a semi-classical approximation is used here.

The classical equation governing the distribution function f is [24]

$$\left(\frac{\boldsymbol{p}}{m}\cdot\nabla_r-(\nabla_rV)\cdot(\nabla_p)+\frac{\partial}{\partial t}\right)f(\boldsymbol{r},\boldsymbol{p}) =\mathcal{I}(\boldsymbol{r},\boldsymbol{p})-G(\boldsymbol{r})f(\boldsymbol{r},\boldsymbol{p}). \tag{68}$$

The left-hand side describes the motion of the atoms in the potential $V(\boldsymbol{r})$. Because atoms in a trap are not flowing as a mass, it can be simplified considerably as will be seen shortly. The right-hand side reflects collision processes. The elastic term $\mathcal{I}$ is given by

$$\mathcal{I}(\boldsymbol{r},\boldsymbol{p}_1)=\frac{2\pi}{\hbar}\frac{|T^{2B}|^2}{(2\pi\hbar)^6}\int\mathrm{d}^3p_2\,\mathrm{d}^3p_3\,\mathrm{d}^3p_4 \times\delta^3(\boldsymbol{p}_1+\boldsymbol{p}_2-\boldsymbol{p}_3-\boldsymbol{p}_4)\delta(E_1+E_2-E_3-E_4) \times[f(\boldsymbol{r},\boldsymbol{p}_3)f(\boldsymbol{r},\boldsymbol{p}_4)-f(\boldsymbol{r},\boldsymbol{p}_1)f(\boldsymbol{r},\boldsymbol{p}_2)], \tag{69}$$

with $E_i=p_i^2/2m$ and T^{2B} being the T-matrix defined in section 2. This is essentially an expression of Fermi's golden rule for a transition from two particles with momentum $(\boldsymbol{p}_3,\boldsymbol{p}_4)\rightarrow(\boldsymbol{p}_1,\boldsymbol{p}_2)$ and the reverse. The population $f(\boldsymbol{r},\boldsymbol{p}_1)$ increases when two atoms with momenta $\boldsymbol{p}_3$ and $\boldsymbol{p}_4$ collide and one acquires momentum $\boldsymbol{p}_1$, and the population decreases when an atom with momentum $\boldsymbol{p}_1$ collides and acquires a new momentum. The transition rates are summed over the three other momenta involved, with the delta functions conserving energy and momentum and expressing the density of states. The T-matrix is, as noted in the discussion following

equation (35), the matrix element for an atom to make a transition between momentum states. In the low-energy limit, it is a constant and is taken outside the integral. The factors of $\hbar$ and 2π provide the correct normalization for the integral. Substituting the value of T^{2B} and simplifying, the prefactor becomes

$$\frac{1}{8\pi^4}\frac{4\pi|a|^2}{m^2\hbar^3}, \tag{70}$$

where the expression $4\pi a^2$ is recognized as the s-wave collisional cross section σ. As discussed in section 2.1, the cross section is enhanced by a factor of two for a Bose gas, and the same factor must be applied to (69). The correct prefactor is therefore

$$\frac{\sigma}{8\pi^4 m^2\hbar^3}, \tag{71}$$

with $\sigma = 8\pi a^2$.

The second term in (68) represents losses from the trap, and is given by

$$G(\boldsymbol{r}) = G_1 + \frac{2G_2}{(2\pi\hbar)^3}\int \mathrm{d}^3p\; f(\boldsymbol{r},\boldsymbol{p}). \tag{72}$$

Here G_1 accounts for density-independent losses due to collisions with background-gas atoms, and G_2 is the rate for dipolar relaxation collisions, as in (64). In our experiment, three-body molecular recombination is only important in the case of a collapsing condensate. Loss due to background gas is generally negligible as well, but its inclusion is trivial.

If f is to represent a Bose gas, it is necessary to include the stimulated scattering factors discussed in section 1.2. A genuine derivation of these factors and the correctness of the QBE in general is beyond the scope of this work [55]. However, the Bose factors are a simple extension to the classical equation, modifying $\mathcal{I}$ to

$$\begin{aligned}\mathcal{I}(\boldsymbol{r},\boldsymbol{p}_1) = {}& \frac{\sigma}{4\pi^4 m\hbar^3}\int \mathrm{d}^3p_2\,\mathrm{d}^3p_3\,\mathrm{d}^3p_4 \\ & \times\delta^3(\boldsymbol{p}_1+\boldsymbol{p}_2-\boldsymbol{p}_3-\boldsymbol{p}_4)\,\delta(p_1^2+p_2^2-p_3^2-p_4^2) \\ & \times[f_3f_4(1+f_1)(1+f_2)-f_1f_2(1+f_3)(1+f_4)].\end{aligned} \tag{73}$$

The QBE is a nonlinear seven-dimensional partial integro-differential equation, and its numerical solution is a substantial computational challenge. A convenient simplifying approach is to assume that the motion of atoms in the trap is ergodic [56, 57]. This means that an atom with a given energy is equally likely to be found at any accessible point in phase space, and that the motions of different atoms are uncorrelated. This excludes collective motions of the gas as a whole, such as pulsating, swirling or sloshing back and forth in the trap. However, such motions are not driven in the experiment, and any motion created, perhaps when the trap is loaded, would be rapidly damped by collisions and by the trap anisotropy. The ergodic approximation has been numerically justified by Monte Carlo simulations of trapped atom distributions, both by ourselves and others [58, 59].

Mathematically, the ergodic approximation means that the distribution function $f(\boldsymbol{r},\boldsymbol{p})$ depends only on the energy $H(\boldsymbol{r},\boldsymbol{p}) = p^2/2m + V(\boldsymbol{r})$. In general, the energy distribution function $f(E)$ is defined by

$$g(E)f(E) = \frac{1}{(2\pi\hbar)^3}\int \mathrm{d}^3r\,\mathrm{d}^3p\;\delta(E-H(\boldsymbol{r},\boldsymbol{p}))f(\boldsymbol{r},\boldsymbol{p}), \tag{74}$$

so that the number of atoms with energy E is

$$\mathrm{d}N = g(E)\,f(E)\,\mathrm{d}E, \tag{75}$$

with density of states $g(E)$. For a harmonic oscillator potential $V(\boldsymbol{r}) = m(\omega_x^2x^2+\omega_y^2y^2+\omega_z^2z^2)/2$, the density of states is

$$g(E) \equiv \frac{1}{(2\pi\hbar)^3}\int \mathrm{d}^3r\,\mathrm{d}^3p\;\delta(E-H(\boldsymbol{r},\boldsymbol{p})) = \frac{E^2}{2(\hbar\omega)^3}, \tag{76}$$

where $\omega \equiv (\omega_x\omega_y\omega_z)^{1/3}$. The ergodic approximation consists of the assumption that

$$f(\boldsymbol{r},\boldsymbol{p}) = \int \mathrm{d}E\,\delta(H(\boldsymbol{r},\boldsymbol{p})-E)\,f(E). \tag{77}$$

The equation governing $f(E)$ is found by multiplying the QBE by $\delta(E-H(\boldsymbol{r},\boldsymbol{p}))$ and integrating over $\boldsymbol{r}$ and $\boldsymbol{p}$. The result is

$$g(E)\frac{\partial f(E)}{\partial t} = \mathcal{I}(E) - G(E)g(E)f(E). \tag{78}$$

The flow terms on the left-hand side of (68) cancel, the collision integral becomes

$$\begin{aligned}\mathcal{I}(E_1) = {}& \frac{m\sigma}{\pi^2\hbar^3}\int \mathrm{d}E_2\,\mathrm{d}E_3\,\mathrm{d}E_4\;g(E_{\min}) \\ & \times\delta(E_1+E_2-E_3-E_4) \\ & \times[f_3f_4(1+f_1)(1+f_2)-f_1f_2(1+f_3)(1+f_4)],\end{aligned} \tag{79}$$

and the loss rate is

$$\begin{aligned}G(E) = {}& G_1 + G_2(2m)^{3/2}\left(\frac{2}{\pi\hbar}\right)^3\int_0^\infty \mathrm{d}E'\,\frac{E_<^{5/2}}{E^2} \\ & \times h\left(\frac{E_>}{E_<}\right)\,f(E').\end{aligned} \tag{80}$$

The energy $E_{\min} = \min\{E_1, E_2, E_3, E_4\}$, and $E_<$ is the lesser of E and E'. The function h is the definite integral

$$h(x) = \int_0^1 \mathrm{d}z\,z^2\sqrt{1-z^2}\sqrt{x-z^2}, \tag{81}$$

well defined for $x > 1$.

The derivation of (80) is straightforward. It is useful to note that the integral over $\boldsymbol{r} = (x, y, z)$ can be transformed to an integral over $\boldsymbol{s} \equiv (\omega_x x, \omega_y y, \omega_z z)$, which restores spherical symmetry to the anisotropic problem. The function h cannot be reduced to closed form, but must be evaluated numerically.

In comparison, the simplicity of expression (79) is a truly remarkable result. Its derivation, however, is more subtle, and for this reason is presented here (see also [56]). The expression obtained directly from (73) is

$$\begin{aligned}\mathcal{I}(E_1) = {}& \frac{A}{(2\pi\hbar)^3}\int \mathrm{d}E_2\,\mathrm{d}E_3\,\mathrm{d}E_4\;\Upsilon(E_1,E_2,E_3,E_4) \\ & \times\int \mathrm{d}^3r\,\mathrm{d}^3p_1\ldots\mathrm{d}^3p_4\;\delta^3(\boldsymbol{p}_1+\boldsymbol{p}_2-\boldsymbol{p}_3-\boldsymbol{p}_4) \\ & \times\delta(p_1^2+p_2^2-p_3^2-p_4^2)\prod_{i=1}^4\delta\left(\frac{p_i^2}{2m}+V(\boldsymbol{r})-E_i\right).\end{aligned} \tag{82}$$

The function Υ contains the factors of f, all of which have been expressed in terms of energy using (77). The prefactor of (73) is abbreviated A. Consider first the spatial and

momentum integrals, which are completely symmetric in the $\boldsymbol{p}_i$ and E_i. The variables can therefore be relabelled to make $E_1 = \min\{E_i\}$, so that for fixed $\boldsymbol{r}$, p_1 will be the smallest of the p_i. The integrals can then be rearranged as

$$\begin{aligned}\int \mathrm{d}^3r\,\mathrm{d}^3p_1\ \delta\left(\frac{p_1^2}{2m}+V(\boldsymbol{r})-E_1\right)\\ \times\frac{1}{2m}\delta(E_1+E_2-E_3-E_4)\\ \times\int \mathrm{d}p_2\,\mathrm{d}p_3\,\mathrm{d}p_4\ p_2^2\,p_3^2\,p_4^2\prod_{i=2}^{4}\delta\left(\frac{p_i^2}{2m}+V(\boldsymbol{r})-E_i\right)\\ \times\int \mathrm{d}^2\Omega_2\,\mathrm{d}^2\Omega_3\,\mathrm{d}^2\Omega_4\ \delta^3(\boldsymbol{p}_1+\boldsymbol{p}_2-\boldsymbol{p}_3-\boldsymbol{p}_4). \qquad (83)\end{aligned}$$

The integral over the solid angles is evaluated as

$$\begin{aligned}&\int \mathrm{d}^2\Omega_2\,\mathrm{d}^2\Omega_3\,\mathrm{d}^2\Omega_4\ \delta^3(\boldsymbol{p}_1+\boldsymbol{p}_2-\boldsymbol{p}_3-\boldsymbol{p}_4)\\ &=\int \mathrm{d}^2\Omega_2\,\mathrm{d}^2\Omega_3\,\frac{1}{p_4^2}\delta(p_4-|\boldsymbol{p}_1+\boldsymbol{p}_2-\boldsymbol{p}_3|)\\ &=\frac{4\pi}{p_4}\int \mathrm{d}^2\Omega_2\int \mathrm{d}\theta_3\ \sin\theta_3\\ &\quad\times\delta(p_4^2-P^2-p_3^2+2Pp_3\cos\theta_3), \qquad (84)\end{aligned}$$

with P defined to be $|\boldsymbol{p}_1+\boldsymbol{p}_2|$ and θ_3 taken as the angle between $\boldsymbol{p}_3$ and $\boldsymbol{P}$. For $p_1 = \min p_i$, the delta-function contributes for all angles Ω_2, and the final result is

$$\frac{2\pi}{p_3p_4}\int \mathrm{d}^2\Omega_2\,\frac{1}{|\boldsymbol{p}_1+\boldsymbol{p}_2|}=\frac{8\pi^2}{p_2p_3p_4}. \qquad (85)$$

The last step is elementary, and again relies on p_1 being smaller than p_2. For the remaining integrals in (82), it is necessary only to evaluate the delta-functions in p and recognize the definition of the density of states, yielding

$$\begin{aligned}\mathcal{I}(E_1)=4\pi^2m^2A\int \mathrm{d}E_2\,\mathrm{d}E_3\,\mathrm{d}E_4\ g(E_{\min})\\ \times\delta(E_1+E_2-E_3-E_4)\Upsilon, \qquad (86)\end{aligned}$$

which expands to (79).

Equation (78) is solved as a set of coupled ordinary differential equations in time on a discrete energy grid, so that $f(E) \to f_n$. For a classical gas, the grid spacing is arbitrary, but quantum effects can be included by demanding that the grid spacing $\delta E = j\hbar\omega$, with integer j. Typically, 200 grid points are used, with the highest energy corresponding to roughly $15k_BT$ for a gas at temperature T.

Evaporative cooling is modelled by setting $f(E) = 0$ above a cutoff energy E_T. As the gas cools, the energy grid spacing is dynamically reduced by decreasing j, which is initially on the order of 10^3 for a gas at $T = 200\,\mu$K. The results of the model and its experimental realization are discussed below

After BEC has occurred, it is necessary to account for the instability of the condensate. During a time step $\mathrm{d}t$, the rate for the condensate to collapse is calculated from γ of equations (61) and (62). The temperature of the gas is estimated from the distribution of population in the low-lying levels. A random number x is then chosen, and if $x < \gamma\,\mathrm{d}t$, the condensate is taken to collapse. The collapse occurs instantaneously on the timescale of the QBE, so it is necessary only to know what is left when the collapse is over. As discussed in section 2.2, this issue is currently unclear. Typically, the collapse is assumed to consume the entire condensate, and $f(0)$ is set to zero. Other models can be as easily used, however.

The correct treatment of a degenerate gas requires some care. By setting the minimum-energy point of the grid to the zero-point energy $E_0 = 3\hbar\omega/2$, approximately the right density of states is obtained

$$g(E)\to g_n=\frac{(E_0+n\hbar\omega)^2}{2(\hbar\omega)^3}=\frac{n^2+3n+9/4}{2\hbar\omega}, \qquad (87)$$

where the actual degeneracy in an isotropic harmonic oscillator potential is $(n+1)(n+2)/2$. If the zero-point energy were not included, the condensate population $f(0)$ would be undefined since $g(0)$ would be zero. Also, since f can be large and discontinuous at $n = 0$, the ground state is always treated singly, and not lumped with nearby states when $j > 1$; thus $g(0)$ is always taken to be unity.

It is reasonable to question the validity of the semi-classical approximation for atoms in very low-lying states of the trap. An estimate of the accuracy of the collision rates used can be obtained by calculating the rate for inelastic collisions between condensate atoms, given by $G(0)$. This can be compared with the actual rate determined using the Gaussian ground-state wavefunction. The distribution function for a gas consisting of N_0 atoms at energy E_0 is $f(E) = N_0\,\delta(E - E_0)/g(E_0)$. Using this f, the semi-classical approximation to the loss rate from dipolar decay is found using (80) to be

$$\left.\frac{\mathrm{d}N_0}{\mathrm{d}t}\right|_{\mathrm{sc}}=-\frac{128\sqrt{3}}{135\pi^3}G_2\frac{N_0^2}{\ell_0^3}\approx 0.05G_2\frac{N_0^2}{\ell_0^3}. \qquad (88)$$

Recall that the loss rate is reduced by a factor of 2 due to the coherence properties of the condensate. From (65), the loss rate in the variational quantum calculation is

$$\left.\frac{\mathrm{d}N_0}{\mathrm{d}t}\right|_{\mathrm{q}}=-\frac{1}{(2\pi)^{3/2}}G_2\frac{N_0}{\ell^3}\approx 0.06G_2\frac{N_0^2}{\ell^3}. \qquad (89)$$

For small N_0, mean-field interaction effects are small and $\ell \approx \ell_0$. The error due to the semi-classical approximation is therefore 20%. The collision terms for other low-lying states will be inaccurate by similar but smaller amounts.

Note, however, that for large N_0, mean-field effects become important. For example, ℓ can become significantly smaller than ℓ_0, as seen in figure 3. This leads to a substantial error in the collision terms involving the condensate. In addition, interactions decrease the energy of the condensate appreciably, changing the equilibrium population distribution. Correctly accounting for interactions would require at each time step a self-consistent calculation of the energy spectrum and collision rates. This would comprise a substantial theoretical effort, which has yet to be fully achieved [60, 61]. A discussion of some of the effects which might be expected is given in section 3.2. Otherwise, the model used here can provide only a qualitative description of the expected behaviour at large N_0.

Another numerical technique for solving the QBE is the Monte Carlo method, in which the gas is represented by several

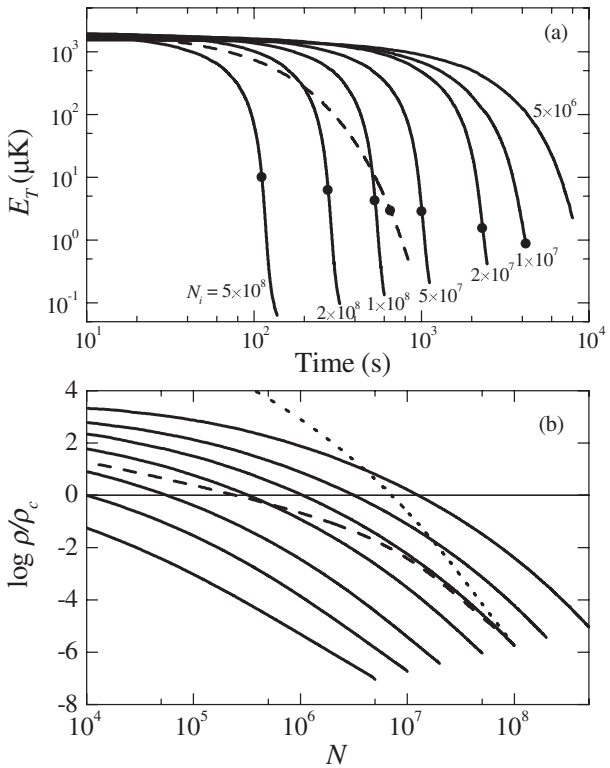

Figure 9. Optimized evaporative cooling trajectories. (*a*) Solid curves are optimized values of $E_T(t)$ for the initial values of N shown. The initial temperature is 500 μK in each case. Dots show the time at which BEC would be reached, if the Bose stimulation factors were included in the calculation. (*b*) Response of the gas to the cooling trajectories in (*a*). The phase-space density is shown in terms of the critical point for BEC, $\varrho = 1$. The long-dashed curves show a typical unoptimized trajectory for comparison. For these calculations, $G_1 = 10^{-4}$ s^{-1} and $G_2 = 10^{-14}$ cm^3 s^{-1} [65]. The dotted curve shows the cooling achieved when $G_2 = 10^{-15}$ cm^3 s^{-1}.

thousand model atoms whose trajectories and interactions are calculated by various approximation schemes [58, 59, 62, 63]. Averaging of the states of the model atoms then gives the thermodynamic properties of the gas, to some degree of precision. This allows, for example, relaxation of the ergodic approximation, and might more easily permit the incorporation of mean-field interactions. A direct comparison of calculation speeds is not available, but typically Monte Carlo methods are slow.

3.2. Model results

The QBE is first applied to the simulation of evaporative cooling, an essentially classical phenomenon. Evaporative cooling has been generally described in [64], so it is summarized only briefly here. The QBE is then applied to the problem of BEC and the ensuing dynamics.

Evaporative cooling requires a mechanism to selectively remove atoms from the trap based on their energy. As discussed in section 1.2, the atoms are confined only if their magnetic moment $\boldsymbol{m}$ is anti-parallel to $\boldsymbol{B}$. Atoms can therefore be removed by driving a transition between a trapped and untrapped spin state using an oscillating transverse field. If the untrapped state experiences a repelling potential energy $V^*(\boldsymbol{r})$, then the energy difference $V(\boldsymbol{r}) - V^*(\boldsymbol{r})$ has a strong spatial dependence, and increases with r. An applied field with frequency Ω_T will be resonant only at positions where $V(\boldsymbol{r}) - V^*(\boldsymbol{r}) = \hbar\Omega_T$. Atoms with energy $E < V(\boldsymbol{r})$ will never be found at such $\boldsymbol{r}$, and thus will remain trapped, while atoms with greater energies will be lost. In this way, Ω_T defines the depth of the trap E_T.

The trap depth is typically set to be two to three times higher than the average energy of the atoms in the cloud, where $\langle E\rangle = 3k_BT$. When the oscillating field is imposed, $\langle E\rangle$ immediately decreases, and as elastic collisions attempt to repopulate the missing tail of the distribution, cooling continues. As $\langle E\rangle$ decreases, E_T is lowered to keep pace. If E_T is reduced too quickly, too many atoms are lost for the amount of cooling produced, but if E_T changes too slowly, atoms are lost due to background-gas collisions and dipolar relaxation.

We perform evaporative cooling on a sample of $\sim 2 \times 10^8$ ^{7}Li atoms loaded into the magnetic trap and laser cooled to a temperature of $\sim$250 μK. The atoms are held in the ($F = 2$; $m_F = 2$) doubly spin-polarized hyperfine state, and are driven to the ($F = 1$; $m_F = 1$) untrapped state. The magnetic field at the centre of the trap is 10^3 G, and the frequency of the spin-flip transition is approximately 3.4 GHz. The microwave field is obtained from a digital frequency synthesizer, and applied to a 2 cm diameter loop antenna placed $\sim$2.5 cm from the trap centre. Roughly 100 mW of microwave power is applied to the antenna, of which an estimated half is coupled into the trap chamber. The frequency Ω_T is initially 70 MHz above the trap-bottom resonance, and is gradually reduced. BEC is reached after approximately three minutes of cooling, when Ω_T is approximately 150 kHz above the trap bottom, $N \approx 10^6$ atoms, and $T \approx 700$ nK. We use an optimized trajectory $\Omega_T(t)$ [52], which is important both because it increases the temperature and number of atoms at which BEC occurs and because it decreases the cooling time required. Examples of the calculated trajectories are shown in figure 9, for a variety of initial conditions. For these trajectories the Bose stimulation factors ($1+f_i$) were artificially suppressed to demonstrate the predicted behaviour of a classical gas.

Having addressed the technical issue of producing a quantum degenerate gas using evaporative cooling, we now apply the quantum Boltzmann model to BEC itself. Of particular interest are the effects of having the condensate collapse, and the kinetics of condensate formation. It is also useful to characterize the nonequilibrium distributions observed in the model.

If the condensate did not collapse, then evaporative cooling would produce results such as those shown in figure 10(*a*). The BEC phase transition is clearly seen as a rapid jump in condensate number. The subsequent decline in N_0 is caused by dipolar-relaxation collisions in the relatively dense condensate. This is not a quantitatively accurate model of the behaviour of a gas with $a > 0$, because it neglects mean-field interactions, which become important for large N_0 [60]. Qualitatively, however, the picture is correct. In contrast, when collapses are included they yield the behaviour shown in figure 10(*b*). Roughly 150 cycles of condensate growth and collapse occur, finally ceasing when the total number of trapped atoms N drops too low to allow further cooling.

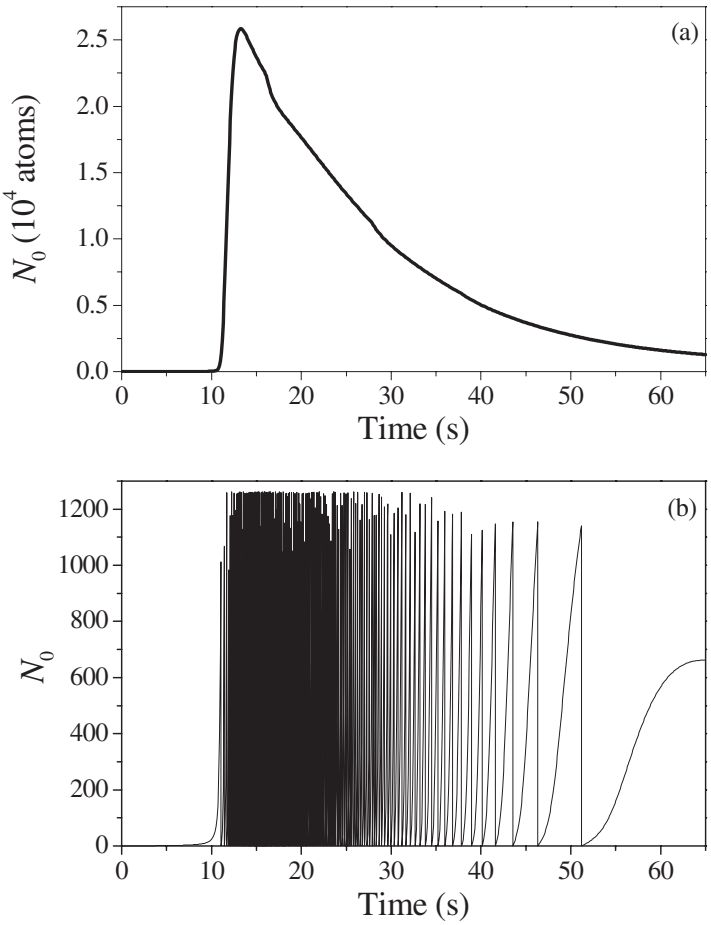

Figure 10. Modelling BEC with the quantum Boltzmann equation. (*a*) Behaviour obtained when the instability of the condensate is disregarded. (*b*) Behaviour when collapses are included and assumed to reduce N_0 to zero. For both plots, the gas is initially in a nondegenerate equilibrium distribution with $N = 4.5 \times 10^6$ atoms at $T = 2.1\ \mu$K. Evaporative cooling is applied with parameters simulating those used in the experiments described in section 4.

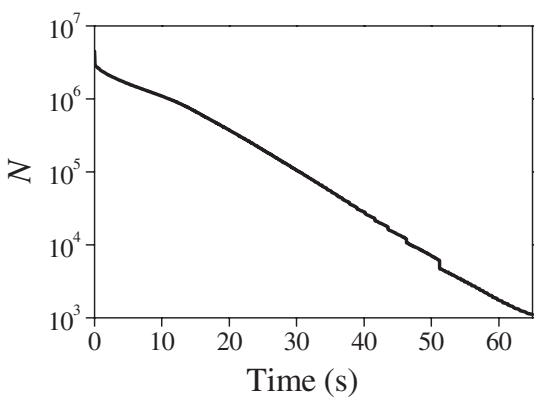

Figure 11. Loss of atoms during evaporative cooling of a degenerate gas. The total number of trapped atoms N corresponding to the curve of figure 10(*b*) is shown. Until the very final stages of cooling, $N \gg N_0$.

A plot of $N(t)$ is shown in figure 11. In the experiments to be described, condensates can be observed most accurately when $N < 5 \times 10^4$, so the final portion of the time range in figure 10 is usually the focus of attention.

The details of the behaviour seen in figure 10(*b*) depend on the collapse model used. As discussed in section 2.3, there is no generally accepted theoretical prediction for the number of atoms left in the condensate after a collapse. It was assumed for the figure that the entire condensate is eliminated, but other models can also be applied. Figure 12 shows the results obtained when it is assumed (*a*) that the collapse leaves half the atoms behind, and (*b*) that the collapse leaves a variable number of atoms, with a probability distribution

$$P_R(N_0) = A \exp\left[-\frac{(N_0 - N_R)^2}{w^2}\right], \qquad (90)$$

with $N_R = 200$ atoms and $w = 100$ atoms. Of these possibilities, figure 12(*b*) agrees best with the experimental evidence, as will be discussed in chapter 4. However, all three predict qualitatively similar behaviour, in that N_0 oscillates between some minimum and N_m as the condensate alternately fills and collapses.

It is interesting to note that the last collapse in the trajectories of figures 10(*b*) and 12(*a*) and (*b*) all occur at nearly the same time. In part, this can be explained because the atoms lost in the collapses make up only about 20% of the total loss in N, so that the kinetics are mainly determined by losses from evaporative cooling and dipolar relaxation. Furthermore, the total number of atoms lost in collapses is very similar in all three cases, $1.95 \pm 0.01 \times 10^5$ atoms. Clearly, atoms are driven

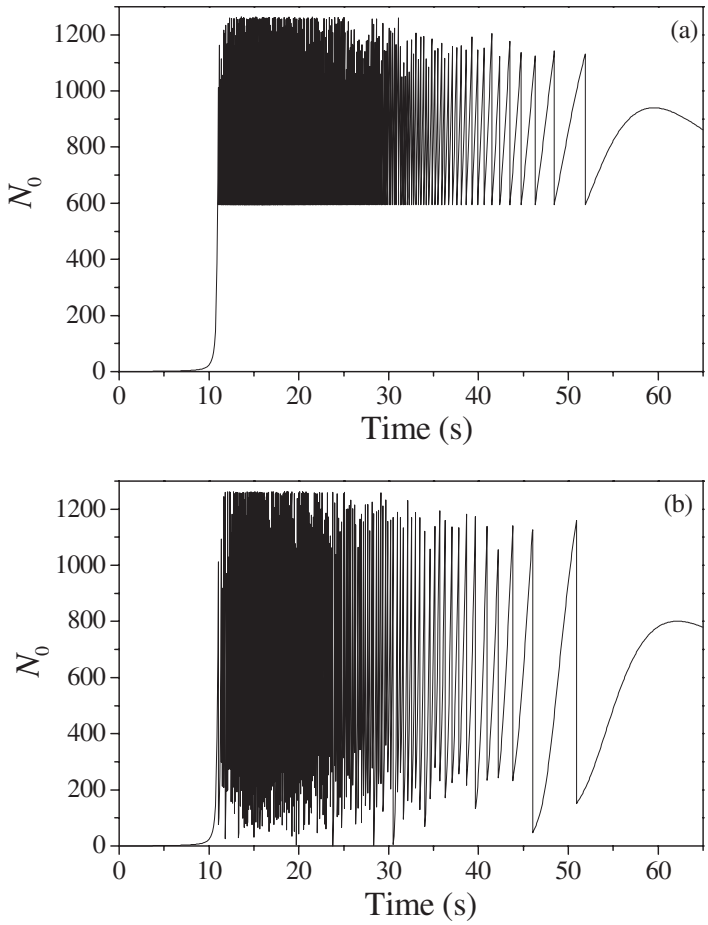

Figure 12. Alternative collapse models. The simulations of figure 10 are repeated assuming that (*a*) each collapse reduces N_0 to $N_m/2$, as proposed by Kagan *et al*, and (*b*) that a collapse leaves behind a random number of atoms according to a Gaussian distribution (90).

into the condensate at an average rate which is fundamentally fixed by the evaporative cooling process and independent of the detailed condensate dynamics.

The dynamics of N_0 also depend on the initiation of the collapse by thermal fluctuations. Because of this stochastic element, there is a dephasing of the collapse/fill cycles. If an identical trajectory is simulated twice with different random number generation sequences, the results eventually become uncorrelated. Typically this takes about 40 collapses in the QBE model, corresponding to roughly 5 s in figure 10. In principle, a measurement of this decorrelation time under various conditions could provide information about the initiation process. However, $N_0(t)$ is also quite sensitive to experimental variations in the temperature and number of atoms at the beginning of evaporative cooling. A 10% variation in the initial number of atoms shifts the time of the first collapse by $\sim$2 s. So, if the dephasing due to thermal fluctuations is to be observed, the trap loading process must be well controlled. In any case, it is clear that once many collapses have occurred, the value of N_0 at a particular time will be unpredictable.

In figure 10, the gas is never in equilibrium, since evaporative cooling is taking place. To exhibit the equilibration process itself, cooling can be halted and the gas allowed to evolve freely. An example of the response is shown in figure 13. Inelastic collisions in the gas and in the condensate cause N to decrease and T to rise, lowering the phase-space density ϱ and slowing down the rate at which atoms enter the condensate. Eventually, the gas comes to equilibrium with some $N_0 < N_m$, after which time N_0 decreases as ϱ continues to drop. In figure 13, equilibration occurs 40 s after the cooling perturbation.

This equilibration time is surprisingly long. The mean collision rate for the conditions shown is approximately 0.5 Hz, so that each atom collides 20 times on average before N_0 stops increasing. This indicates that it is unlikely for an average collision to produce a condensate atom, even though the rate for this process is enhanced by a factor of N_0. If the condensate number were not limited so that N_0 could be larger, equilibration would be much faster, although the higher condensate density in this case also increases the loss rate and makes direct comparison difficult. Equilibration is also faster in a nondegenerate gas, requiring only $\sim$5 collisions per atom.

The relatively slow equilibration of a degenerate gas indicates that an average collision is unlikely to produce a condensate atom. This can be understood from the fact that the volume of the condensate in phase space is very small. A collision giving an increase in N_0 must take place at the very centre of the cloud, and between two relatively cold atoms. This statement can be quantified using (79), which gives the rate for any particular collision process. The rate of increase

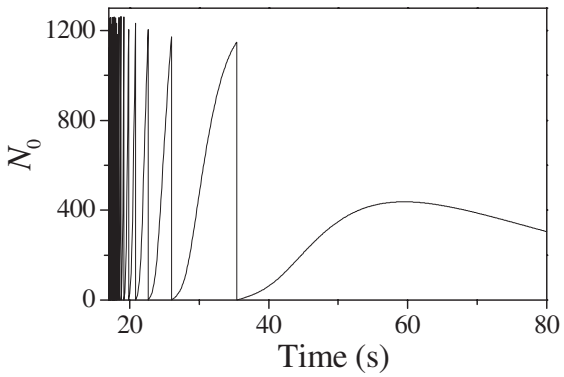

Figure 13. Modelling equilibration. Evaporative cooling is simulated as in figure 10(*b*), but at $t = 17.6$ s, E_T is abruptly lowered to 12 kHz = 500 nK. Cooling is then halted and the gas allowed to equilibrate. This corresponds to the experimental procedure used in section 4.

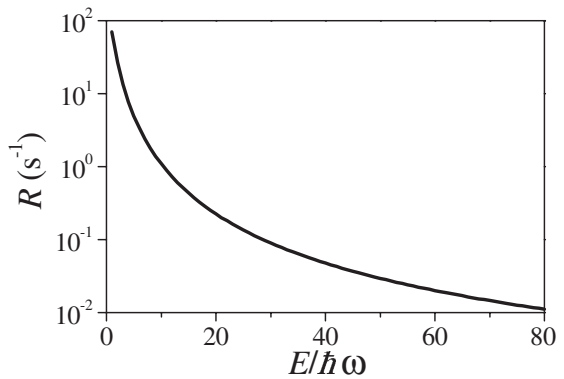

Figure 14. Rate R_0 for atoms to enter condensate, as a function of level energy E. From (93), for $N_0 = 1000$ atoms and $T = 150$ nK.

of the condensate population is

$$g(E_0)\frac{\mathrm{d}f(E_0)}{\mathrm{d}t} = Ag(E_0)\int \mathrm{d}E_3\,\mathrm{d}E_4\, f(E_3)f(E_4)[1+f(E_0)] \times[1+f(E_3+E_4-E_0)], \tag{91}$$

which for $N_0 \gg 1$ can be expressed as

$$\frac{\mathrm{d}N_0}{\mathrm{d}t} = N_0\int \mathrm{d}E\, g(E)f(E)R_0(E), \tag{92}$$

where $R_0(E)$ is the rate at which an atom with energy E is likely to enter the condensate. It is given by

$$R_0(E) = \frac{A}{g(E)}\int \mathrm{d}E'\, f(E')[1+f(E+E')], \tag{93}$$

and is plotted in figure 14 for an equilibrium gas. It does indeed decrease quickly as a function of E, indicating that most of the atoms entering the condensate come from a relatively small number of low-lying energy levels.

This argument suggests the three-state picture shown in figure 15. The upper level $|b\rangle$ represents the majority of the trapped states, which are not well connected to the condensate state $|0\rangle$. Instead, they are weakly connected to a group of low-lying states represented by $|a\rangle$. The γ_{ij} parameters describe the coupling between levels, with

$$\gamma_{ab} \ll \gamma_{0a}. \tag{94}$$

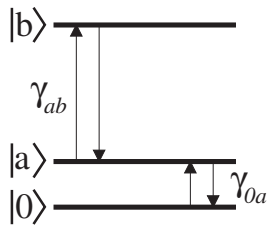

Figure 15. Three-level model of condensation process. Level $|0\rangle$ represents the condensate, level $|a\rangle$ a group of low-lying states and $|b\rangle$ the majority of the occupied states of the trap. Population is transferred between levels at the rates γ_{ij}.

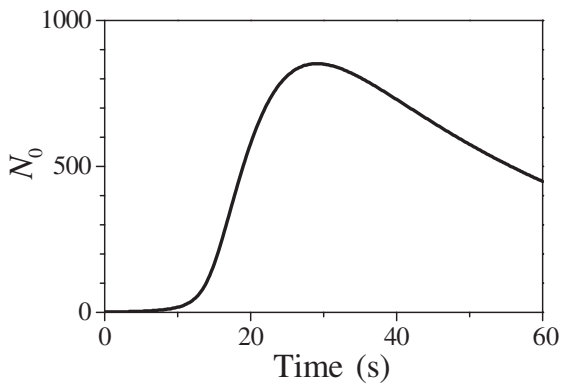

Figure 16. Initiation of BEC. A nondegenerate gas initially at $T = 500$ nK with $N = 2.2 \times 10^5$ atoms is cooled at $t = 0$ by removing all atoms having $E > T$. The gas then freely evolves, undergoing BEC at $t \approx 10$ s.

Because of their strong coupling, the populations of states $|0\rangle$ and $|a\rangle$ are always close to equilibrium. The population N_a therefore saturates at some level given by the Bose–Einstein distribution, with any excess atoms rapidly entering the condensate. Because of this saturation, the Bose enhancement of γ_{ab} never gets very large.

This picture of the filling process explains many aspects of the condensate dynamics. For instance, figure 16 shows the response of an initially nondegenerate gas when evaporative cooling is suddenly applied. At $t = 0$, all atoms with energy greater than T are removed, and the gas is then allowed to equilibrate. As can be seen, there is an appreciable delay before condensation occurs. This delay can be understood as the time required for enough population to be transferred from the high-lying energies $|b\rangle$ to saturate the states $|a\rangle$. Once this occurs, N_0 starts to grow.

The picture also explains the shape of $N_0(t)$ following a collapse, as seen in figures 10 and 12. An expanded view is shown in figure 17. There are two phases to this filling process. The condensate first must come to equilibrium with the low-lying states $|a\rangle$. The transfer rate γ_{0a} depends strongly on N_0 through the Bose stimulation factor, so this process accelerates as the condensate fills. However, once equilibrium between $|0\rangle$ and $|a\rangle$ is established, the growth in N_0 levels out. In figure 17, this occurs at $N_0 \approx 200$ atoms. After this point, N_0 grows linearly, reflecting the constant addition of atoms to the $|0\rangle$–$|a\rangle$ subsystem from $|b\rangle$. If the gas as a whole is approaching equilibrium, γ_{ab} itself decreases, causing the condensate growth to slow and correspondingly slowing

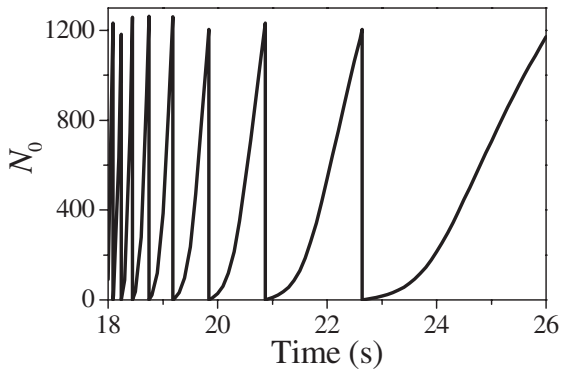

Figure 17. Filling curve. An expanded view of a portion of figure 13, showing the shape of $N_0(t)$ after a collapse.

down the collapse/fill cycle. This can be seen in the long-time behaviour of figure 13.

Recall, however, the discussion at the end of section 3.1, noting that the QBE model neglects important mean-field interaction effects when N_0 is large. In particular, as the condensate fills, E_0 decreases, which shifts the equilibrium between the $|0\rangle$ and $|a\rangle$ states. This should cause the condensate to fill faster than the QBE predicts. An estimate of the size of the effect can be made by considering the shift in the equilibrium population of the condensate due to the interaction energy. In equilibrium, the population of each quantum state is given by the Bose–Einstein distribution

$$f(E) = \frac{1}{\exp[(E-\mu)/k_{\mathrm{B}}T] - 1}, \tag{95}$$

where the chemical potential μ satisfies

$$\mathrm{e}^{-\beta\mu} = 1 + \frac{1}{N_0} \tag{96}$$

when the ground-state energy E_0 is taken to be zero. For specified values of N and T, N_0 is found by adjusting μ to give

$$N = \int \mathrm{d}E\, g(E) f(E) \to \sum_n \frac{(n+1)(n+2)}{2} f(E_n). \tag{97}$$

Ordinarily, the energy of the nth excited state is $E_n = n\hbar\omega$, but if interactions lower E_0 by $\delta\hbar\omega$ then the excited-state energies are effectively raised, to

$$E_n = (n+\delta)\hbar\omega. \tag{98}$$

Just before the condensate collapses, the energy shift obtained from (50) is $0.4\hbar\omega$. Comparing the determinations of N_0 with and without this δ indicates that the interactions increase N_0 by ∼350 atoms at $T = 150$ nK and $N = 1.44 \times 10^4$. This is a significant effect, since it is a sizable fraction of N_m. It is, however, only an upper bound since interactions will lower the energy of the excited states as well. The equilibrium effect could be calculated accurately using the methods of [39] or [40].

An accurate calculation of the dynamical effect of this interaction energy is more difficult, for the reasons previously discussed. An attempt was made to use the three-level system

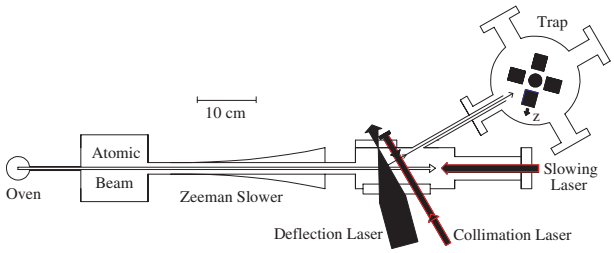

Figure 18. Schematic diagram of experimental apparatus.

as an approximate model, and indicated that the interaction shift causes roughly a 20% increase in the condensate fill rate for large N_0. However, the quantitative accuracy of the three-level model is questionable. In particular, the choice of energy level splittings required to reproduce the filling curve of figure 17 gives a substantially smaller equilibrium population shift than that calculated above. This suggests that the dynamical effect may in reality be somewhat larger.

4. Experimental results

The previous sections have depicted a condensate with $a < 0$ as a highly dynamical object, with violent collapses interspersed among periods of growth. We wish to experimentally observe as many aspects of this behaviour as possible. Previous work has demonstrated that the condensate occupation number is limited to a value in agreement with predictions [66], and in this section observations relating to the dynamics of the condensate are described. Owing to the difficulty of making precise measurements on samples of a thousand atoms or less, these observations are perforce indirect. Nonetheless, a wealth of information is obtained, which both qualitatively confirms the predictions of the theory and points out limitations in its quantitative accuracy.

The experimental apparatus and procedures are only summarized here, since they are more thoroughly discussed in other works [66–68]. The general techniques of laser slowing and cooling are described at a basic level in [69]. Data and analysis pertaining to our measurements of the distribution of N_0 values are described in detail, as well as a related series of experiments illustrating the equilibration process.

4.1. Apparatus and data acquisition

The experiments reported here were carried out using the same apparatus with which BEC was originally observed in ^{7}Li in 1995, with improvements made to increase repeatability and detection sensitivity. A schematic diagram of the apparatus is shown in figure 18. It consists of two main sections, a slow-atom source and a magnetic trap. The source is based on a laser-slowed atomic beam. A recirculating oven containing a few grams of lithium metal is heated to 600 °C, producing a beam of about 10^{14} atoms s^{-1}.

Atoms in the beam with velocities of about 500 m s^{-1} or less are laser cooled to a velocity of 50 m s^{-1} by a Zeeman slower. Slowing occurs as atoms scatter photons out of a counter-propagating laser beam, and an inhomogeneous magnetic field is used to compensate for the changing Doppler shift of the transition. Approximately 1% of the atoms exiting

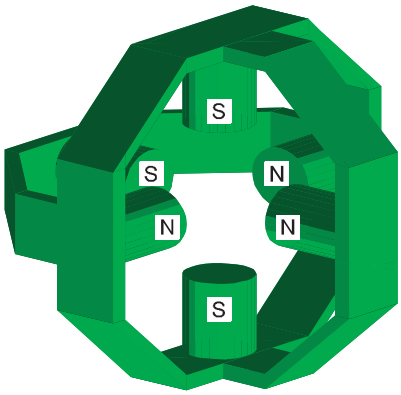

Figure 19. Trap magnet geometry. The cylinders are permanent magnets of the indicated polarity, and the frame is a stainless steel yoke.

the oven are slow enough to be cooled in this way, so the beam emitted from the Zeeman slower is composed of a small low-velocity fraction together with a fast-atom background. These components are separated by a transverse cylindrically focused laser beam. The fast atoms scatter few photons while passing through this beam, while the slow ones are deflected by an angle of 30°. The cylindrically focused laser compensates for the Doppler shift of the atoms as they are deflected, and thus provides a more collimated slow-atom beam. The atoms are further collimated and guided by a set of four laser beams configured as a two-dimensional optical molasses. The atoms enter the trap chamber through a narrow tube, which allows for good differential pumping. *En route*, the atoms are optically pumped into the $(F = 2, m_F = 2)$ hyperfine state.

The trap itself is constructed from six NdFeB-alloy permanent magnets, using the geometry shown in figure 19. The magnets provide a confining field with a minimum of 1000 G and a trap depth of 140 G, or about 10 mK. The trap itself is almost cylindrically symmetric, with atoms oscillating at frequencies of 135.5, 150.6, and 152.6 Hz along its three principal axes. Confinement is weakest in the direction along the magnetic field, which is labelled as z in figure 18. Atoms enter the trapping region and are slowed down to $\sim$1 m s^{-1} by a set of six laser beams, and the atoms are then confined. Loading saturates at an estimated 2×10^8 atoms in a few seconds; this number is probably limited by losses due to optical pumping into untrapped spin states. The atoms are loaded at a temperature of $\sim$0.5 mK using relatively intense laser beams, with $I \sim 40$ mW cm^{-2} per beam. After loading the intensity is reduced by a factor of $\sim$100 for 10 ms, and then ramped off. This cools the atoms to 250 μK, near the Doppler limit of 140 μK. The resonant optical density of the cloud is then 10 or greater, and this high opacity is probably responsible for the inability to achieve the actual Doppler temperature limit.

After the atoms are loaded and cooled, all the laser beams are shut off and the atoms are held purely by magnetic forces. Evaporative cooling is then applied, as described in section 3.2. By continually removing the high-energy tail of the thermal distribution, the atoms are gradually cooled, and after roughly three minutes BEC occurs with $N \approx 10^6$ and $T \approx 700$ nK. In the experiments described here, evaporative cooling is continued until $N \approx 4 \times 10^4$ atoms and $T \approx 150$ nK, which occurs when the evaporative cooling microwave frequency is

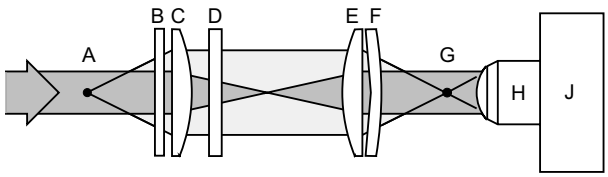

Figure 20. Schematic diagram of imaging system, showing the atom cloud A, vacuum viewport B, achromatic doublets C and E, phase-contrast imaging polarizer D, correction lens F, primary image G, microscope objective H, and CCD camera J. The dark grey area represents the probe beam and the light grey one the coherently scattered light.

about 10 kHz above the trap-centre resonance. The 3.4 GHz microwave frequency must therefore be stable to better than 1 kHz, which is easily achieved using a digital frequency synthesizer. However, the trap magnetic field itself must similarly be stable to better than one part in 10^6, which is more difficult. Since the magnetization of the permanent magnets depends on their temperature, the trap is regulated with heaters and the microwave power used for evaporation is adjusted during cooling to provide a constant heat load. These procedures reduce field fluctuations to $\sim$1 mG, corresponding to a variation in N of $\sim 10^4$ atoms from one repetition of the experiment to the next.

Once a condensate is produced, it is observed using the phase-contrast polarization imaging technique described in [68]. A schematic diagram of the imaging system is shown in figure 20. A probe laser is directed through the cloud and a lens system, onto a CCD camera. The lens system consists of two off-the-shelf achromatic doublets, which relay an image of the cloud outside the vacuum chamber, a custom corrective lens to reduce spherical aberrations and a microscope which magnifies the image onto the CCD. A vacuum viewport is in front of all the lenses, and a polarizer between the doublets is used for phase contrast imaging.

The intensity of the probe beam is reduced as atoms scatter photons out of it, and this absorption can, in principle, be imaged to provide information about the cloud. In addition, the gas as a whole has a substantial index of refraction, so that the light passing through the cloud acquires a phase shift. If the imaging system were perfect, this phase could be ignored, since it would not change the measured intensity. All real lenses, however, will make errors in reconstructing the phase, which cause distortions and reduce the fidelity of the image. To avoid this problem, the probe laser is detuned significantly from resonance, lowering the index of refraction and the corresponding phase shift. Typically, the detuning $\Delta = \pm 40\Gamma$, where $\Gamma = 6$ MHz is the linewidth of the atomic transition. Because the absorption decreases as $1/\Delta^2$ and the index as $1/\Delta$, making the phase shift small enough to avoid imaging distortions makes the absorption too small to observe.

This problem cannot be overcome by simply increasing the probe intensity or the exposure time, since as the atoms scatter photons they are significantly perturbed. For the experiments here, the probe is pulsed on for $\tau_p = 6$ μs with an intensity of 3 W cm^{-2}. During this time each atom scatters about $n_s = 10$ photons, which heats the gas to roughly 20 μK and destroys the condensate. However, during the pulse the

atoms on average move only a distance

$$\delta x = \tfrac{2}{3} v_{\mathrm{R}} \tau_{\mathrm{p}} \sqrt{n_{\mathrm{s}}} \tag{99}$$

transverse to the probe beam, where $v_{\mathrm{R}} = 8.5$ cm s^{-1} is the recoil velocity of a lithium atom. In our case, $\delta x \approx 1$ μm, which is small enough to provide an accurate image.

Because of this limitation, the phase shift caused by the cloud must be imaged directly. This can be achieved in a variety of ways [70,71]. The technique used here relies on the fact that atoms in a large magnetic field are birefringent. The probe laser is tuned near the $(m_J = 1/2, m_I = 3/2) \leftrightarrow (m_J = 3/2, m_I = 3/2)$ transition, so $\Delta m = +1$. The strongest alternative transition is $(m_J = 1/2, m_I = 3/2) \leftrightarrow (m_J = 1/2, m_I = 3/2)$, which is detuned by approximately 1.5 GHz $\approx 250\Gamma$. Therefore, only the σ^+-polarized component of the probe interacts with the atoms, and the scattered and transmitted fields will generally have different polarizations. In our case, the probe polarization is linear with the maximum possible σ^+ projection and the scattered field is elliptically polarized. A polarizer in the lens system projects both fields onto a common axis, so that when the fields recombine in the image plane they interfere, providing an intensity modulation sensitive to the initial phase shift.

The polarization phase contrast system is convenient in several ways. The angle ϑ between the polarizer axis and the probe polarization is readily adjusted, so it can be optimized as experimental conditions vary. The system is also easy to set up, as it is necessary only to add a polarizer to a normal phase-insensitive imaging system. However, it gives a smaller signal than some other imaging techniques, which can be a drawback.

As mentioned, the phase shift ϕ must be kept small to avoid image distortions. In terms of the resonant optical density of the cloud α [27],

$$\phi = \frac{\alpha \Delta / \Gamma}{2I_0/I_{\mathrm{sat}} + 4(\Delta/\Gamma)^2 + 1}, \tag{100}$$

where I_0 is the intensity of the probe and the saturation intensity $I_{\mathrm{sat}} = 10$ mW cm^{-2} for the transition and geometry used. Typical degenerate clouds of 4×10^4 atoms have $\alpha \sim 5$–10, giving $\phi \sim 0.05$ rad for a probe with $\Delta = 40\Gamma$ and $I_0 = 300 I_{\mathrm{sat}}$. In the limit of small ϕ, the signal intensity in the image plane is

$$I_s(r) = I_0 \left[\cos^2\vartheta + \frac{\sqrt{3}}{4}\phi(r)\sin 2\vartheta - \frac{3}{16}\phi(r)^2 \cos 2\vartheta \right], \tag{101}$$

where I_0 is the incident intensity. For the experiments here, $\vartheta = 82.5^\circ$, close to 90° so that the signal-to-background ratio is large, but not so close that the quadratic term in (101) becomes significant. Generally, the reduced signal

$$S \equiv \frac{I_s}{I_0 \cos^2\vartheta} - 1 = \frac{\sqrt{3}}{2}\phi \tan\vartheta \tag{102}$$

is considered, which gives an observable linearly related to ϕ. The background $I_0 \cos^2\vartheta$ is measured separately for each experimental run by taking an additional image after emptying the trap. Since α is related to the density profile of the atoms by

$$\alpha = \sigma_L \int \mathrm{d}z'\, n(\boldsymbol{r}), \tag{103}$$

the signals obtained are direct images of the column density of the cloud. The light-scattering cross section $\sigma_L = 4\pi/k^2$, and the integral is along the propagation direction of the probe beam.

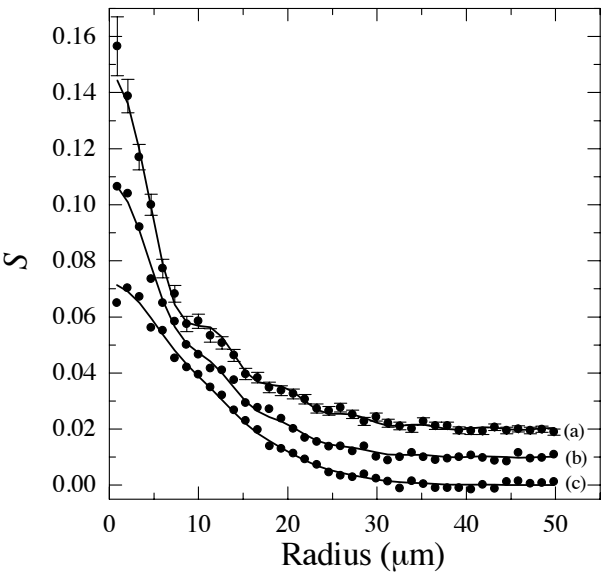

Figure 21. Signal profiles of degenerate clouds, taken 10 s after evaporative cooling was halted. The points represent angular averages of the reduced signal S taken from three different images. The error bars on the upper trace show the estimated uncertainty due to shot noise. The solid curves are fits to the nonequilibrium distribution function (104). For the three traces, the fits give: (a) $N = 1.17 \times 10^4$, $T = 124$ nK, $N_0 = 916$ and $\mathcal{A} = 1.6$, (b) $N = 1.03 \times 10^4$, $T = 106$ nK, $N_0 = 405$ and $\mathcal{A} = 2.3$ and (c) $N = 1.04 \times 10^4$, $T = 108$ nK, $N_0 = 95$ and $\mathcal{A} = 2.3$. For clarity, the signal in trace (a) is offset by 0.02 and in trace (b) by 0.01.

The images obtained are analysed by fitting the observed spatial profiles to a model. Because the gas is not in equilibrium, the images are not well described by the ordinary Bose–Einstein function, but the the QBE model predicts that the energy distribution can be described well by the simple form

$$f(E) = \frac{\mathcal{A}}{\exp[\beta(E-\mu)] - 1} \tag{104}$$

where $\mathcal{A}$, β and μ are fit parameters. At low energies, this function looks much like the ordinary Bose–Einstein distribution, but at high energies it approaches a Boltzmann distribution with chemical potential which can be larger than zero for $\mathcal{A} > 1$. This reflects the fact that, in the nonequilibrium distribution, there is an excess of atoms at high energy which have yet to find their way into the condensate.

The image signals are processed by averaging the two-dimensional images around ellipses of appropriate asymmetry to generate a radial signal profile. Examples are shown in figure 21. Agreement between data and fit is generally good.

The ripples apparent in the upper plot of figure 21 are an artifact of the limited resolution of the imaging system. Neglecting interaction effects, the condensate has a Gaussian

profile with a 1/e-radius of 3.1 μm. The imaging aperture is limited to $f/5.5$ by the vacuum viewport through which the cloud is observed, so a diffraction-limited imaging system would have an Airy spot of radius 4.1 μm. Since the object size is comparable to the resolution, imaging limitations are important, and it is desirable that the lens system be both as ideal and as well characterized as possible. The imaging system used here is similar to that described in [68], but with a different microscope objective and the addition of the corrective lens. The system is nearly diffraction limited, but measurably different.

Aberrations are characterized by the phase error $W(\rho)$ as a function of location on the lens [70,72]. This is the difference in optical path length experienced by a ray passing through the actual lens at position ρ and an ideal lens. The effect of the aberrations on the image is found by convolving the modelled object electric field $\boldsymbol{E}_{\rm obj}$ with the point transfer function, $G(r)$:

$$\boldsymbol{E}_{\rm img}(M\boldsymbol{r}) = \int \mathrm{d}^2 r'\, G(|\boldsymbol{r}-\boldsymbol{r}'|)\, \boldsymbol{E}_{\rm obj}(\boldsymbol{r}'). \tag{105}$$

Here M is the magnification. The point transfer function is simply the Fourier transform of the phase error,

$$G(\boldsymbol{r}) = \frac{1}{(2\pi)^2}\int_\Sigma \mathrm{d}^2 k\, \mathrm{e}^{\mathrm{i}\boldsymbol{k}\cdot\boldsymbol{r}} \exp(\mathrm{i}kW(\boldsymbol{k})), \tag{106}$$

where the wavevector $\boldsymbol{k}$ corresponds to a point on the lens as shown in figure 22. The integral is over the lens aperture Σ, and yields the familiar Airy pattern when $W = 0$. For a cylindrically symmetric system, W can be expanded as

$$W(\rho) = C_2\rho^2 + C_4\rho^4 + C_6\rho^6, \tag{107}$$

where ρ is the distance from a point in the aperture plane to the imaging axis. The phase error can be calculated from knowledge of the lens design, or measured by analysing images of a pointlike object. We determined W on the bench by imaging laser light emitted from a single-mode optical fibre with a $1/\mathrm{e}^2$-intensity radius of 1.7 μm. Analysis of the images yields aberration coefficients of

$$\begin{gathered} C_2 = 0.26\lambda\ \mathrm{cm}^{-2} \qquad C_4 = -0.36\lambda\ \mathrm{cm}^{-4} \\ C_6 = 0.17\lambda\ \mathrm{cm}^{-6} \end{gathered} \tag{108}$$

at best focus. An alternative measurement was made *in situ* by adjusting W to reproduce the observed ripples in images of clouds with large condensates. The resulting values are

$$\begin{gathered} C_2 = 0.34\lambda\ \mathrm{cm}^{-2} \qquad C_4 = -0.30\lambda\ \mathrm{cm}^{-4} \\ C_6 = 0.094\lambda\ \mathrm{cm}^{-6}. \end{gathered} \tag{109}$$

The difference is likely due to additional aberrations caused by the vacuum viewport.

The goal of the above procedure is to determine N_0 as accurately as possible. Fundamentally, the measurement is limited by statistical noise in the CCD camera. For a probe pulse which generates s photoelectrons in a pixel, the shot noise will be $\sqrt{s}$, and this uncertainty can be included in the fitting procedure to determine the resulting uncertainty in the fit parameters. The estimated accuracy of N_0 is then ± 60 atoms.

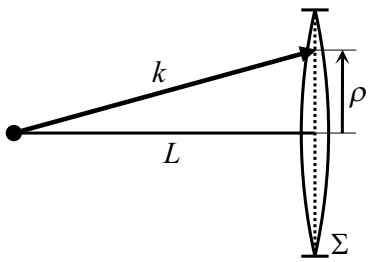

Figure 22. Calculation of point-transfer function. The phase error $W(\boldsymbol{k})$ in (106) is related to the position-dependent phase error $W(\rho)$ as seen above. The lens aperture Σ is located a distance L from the object. The vector labelled k shows the direction of $\boldsymbol{k}$; its magnitude is fixed at $2\pi/\lambda$. The lens position ρ is related to the radial component of $\boldsymbol{k}$ by $\rho = Lk_\rho(k^2 - k_\rho^2)^{-1/2}$.

This is the only source of statistical error in the experiment, in the sense that if two identical atom clouds were imaged and analysed, the only difference in the results would be that caused by variation in the shot noise. The dominant sources of error in the experiment, however, are not statistical but systematic. Chief among these is the uncertainty in the lens aberrations discussed in the previous paragraph. The two different sets of parameters (108) and (109) give N_0 values which differ by about 40%. We assume that the actual aberrations lie somewhere in this range, with an estimated uncertainty of $\pm 20\%$.

Other systematic sources of uncertainty contribute to a lesser degree. From the QBE results, inaccuracy of the nonequilibrium fitting function is expected to lead to an error of ± 75 atoms, but this level of accuracy can only be achieved if the total number of atoms in the cloud is below roughly 5×10^4. Above this range, the N_0 values are artificially inflated. Another source of uncertainty arises from the effect of interactions on the size and shape of the condensate, since this has not been observed experimentally and is not necessarily well understood theoretically. If the compression predicted by the variational model is included, the highest values of N_0 are lowered by about 10%. This provides an estimate of the uncertainty introduced by this variability.

4.2. Distribution of N_0 values

The preceding discussion has illustrated that we can measure N_0 with respectable precision. In order to achieve this, however, it is necessary to destroy the atom cloud as it is being observed, which hinders the study of dynamical properties. As noted in section 3.2, a given trajectory $N_0(t)$ is made unrepeatable by intrinsic quantum and thermal fluctuations, as well as by variations in experimental conditions. This prevents the dynamics from being mapped out by repeating an experiment with a variable delay before probing. Methods to circumvent these limitations can be considered, but the simplest approach is to repeat the experiment many times with a fixed probe delay, and observe the distribution of N_0 values obtained. Since the effect of the experimental and intrinsic fluctuations is to shift the phase of the collapses, this approach effectively averages the probability for a particular N_0 value to occur over the oscillation cycles.

For this experiment, data are obtained by loading atoms into the trap and evaporatively cooling until the microwave

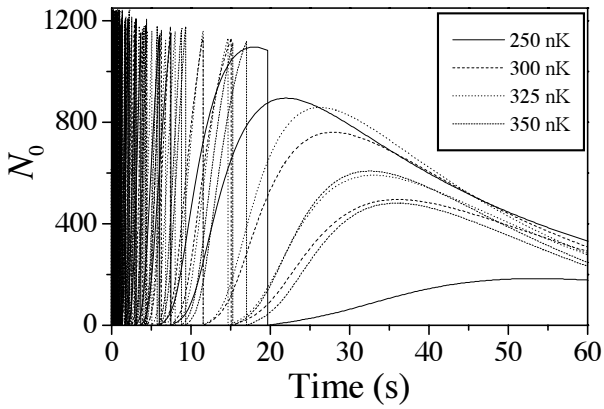

Figure 23. Variations in QBE trajectories. Simulations of the equilibration process such as in figure 13 are repeated with varying random number sequences. The microwave sweep frequencies are also varied to simulate the effect of trap bias field fluctuations. The legend shows the energy to which the trap depth is reduced during the sweep. The time origin is taken to be the time of the sweep.

frequency $\Omega_T \approx 100$ kHz above the trap-centre resonance. Approximately 4×10^5 atoms then remain, at a temperature of ~400 nK. This is well below the point at which BEC typically occurs, to ensure that the gas is in the degenerate regime. In order to accurately determine N_0, N must be further reduced. This is achieved by rapidly sweeping Ω_T down to ~10 kHz and then raising it again. This technique is used because it is fast and because it puts the gas into a definite state at $t = 0$, from which the relaxation to equilibrium can be observed. The microwaves are swept in ~100 ms, quickly compared to the collision rate of about 1 Hz, but slowly compared to the trap oscillation period so that time-of-flight broadening and non-ergodic effects are not important.

After the sweep, roughly 4×10^4 atoms remain trapped, at a temperature of 150 nK. The precise values vary from one repetition to the next because of fluctuations in the trap bias field. The response predicted by the QBE is shown in figure 13, and the variations caused by fluctuations can be seen in figure 23. Collapses continue for 10–20 s after the sweep, equilibrium is reached at $t = 20$–30 s and then the condensate slowly decays because of inelastic collisions.

In the experiment, the gas is allowed to thermalize for a time τ, and is then probed. The results are shown in figure 24. For small τ, N_0 varies from near zero to about 1200 atoms, as expected if the condensate is alternately filling to its maximum and collapsing. At longer time delays, the histograms change shape, narrowing somewhat at $\tau = 30$ s and exhibiting only small N_0 values at $\tau = 60$ s. At each time, the spread in values is much larger than the statistical uncertainty in N_0, so the variations are experimentally significant. This conclusion is confirmed by constructing a histogram at $\tau = 90$ s, when only small N_0 values should occur. As can be seen in figure 25, the results of the measurement are indeed small, and consistent with our expected statistical uncertainty.

This behaviour shown in figures 24 and 25 is qualitatively the same as that seen in figure 23. To our knowledge, no other explanation for variations in N_0 of this magnitude has been proposed, and we consider their observation to strongly support the dynamical picture developed in the previous chapters.

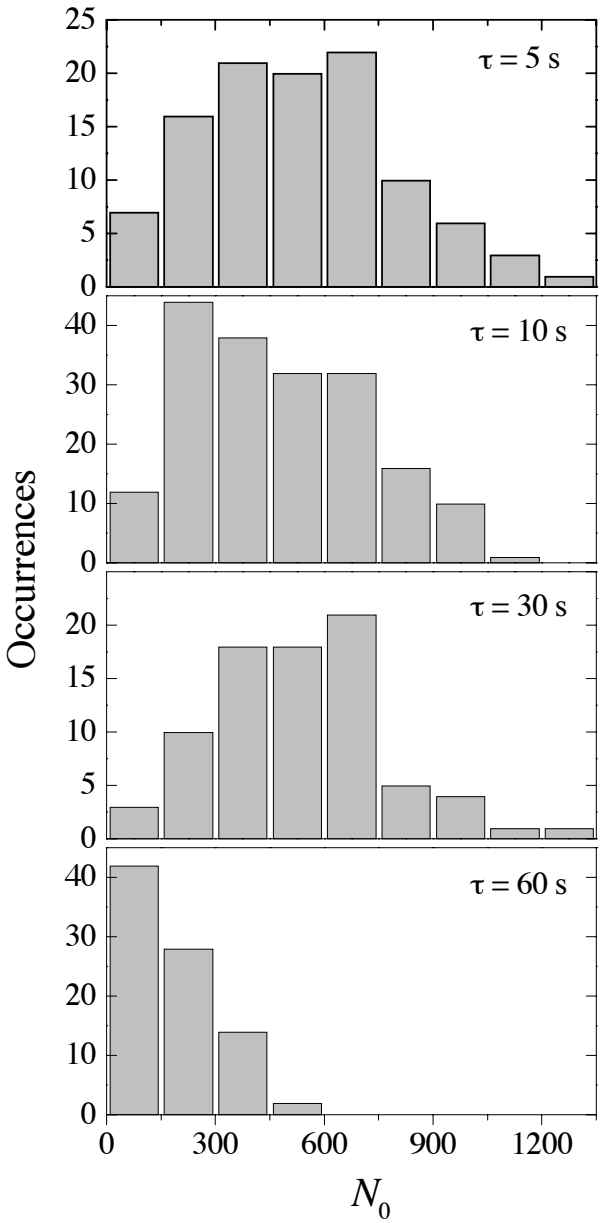

Figure 24. Frequency of occurrence of N_0 values, and dependence on equilibration time τ. The total number of atoms N ranged from 5×10^3 to 3.5×10^4 in each case. The total number of runs is 106 for $\tau = 5$ s, 185 for $\tau = 10$ s, 81 for $\tau = 30$ s, and 86 for $\tau = 60$ s. The width of the bins is approximately the statistical uncertainty in N_0.

Quantitative agreement between the model and data is reasonable, but one notable discrepancy can be observed. In the calculation of figure 23, the collapse was assumed to reduce the condensate number to zero. Immediately after this reduction, N_0 is predicted to grow relatively slowly, so that the values of N_0 most likely to occur are much lower than those seen in figure 24. We interpret this discrepancy to mean that the collapse does not, in fact, remove the entire condensate. As noted in section 2.3, Kagan *et al* [51] predict that the collapse reduces N_0 to $N_m/2$. This possibility is clearly ruled out by the large number of points observed with small N_0. There is, in fact, no fixed value to which the collapse could reduce N_0 which reproduces the observed data, since the probability

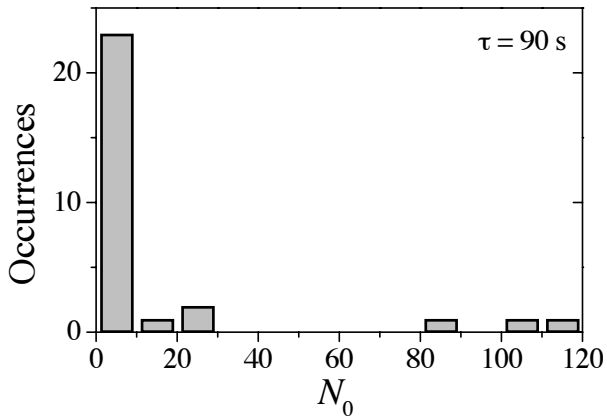

Figure 25. Values of N_0 obtained at $\tau = 90$ s are always small, and consistent with the expected statistical uncertainty in the measurement. A total of 30 runs are shown.

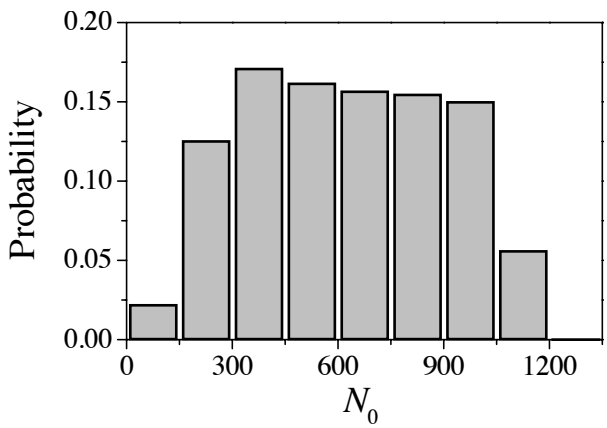

Figure 26. Predicted histogram when collapsing to a Gaussian distribution centred at $N_0 = 200$ atoms and with a $1/e$ half-width of 100 atoms.

of occurrence is seen to rise gradually as N_0 increases from 0 to 200 atoms. The data are described best if the number of atoms remaining after the collapse is allowed to fluctuate, as in figure 12(*b*). The predicted histogram for this case is shown in figure 26, and agrees reasonably well with the data for short τ.

At longer delay times, quantitative comparison with theory is difficult because the N_0 values predicted by the QBE model depend sensitively on the time at which the last collapse occurs. However, from the simulation data shown in figure 23, the model appears to be reasonably consistent with the measured distribution at $\tau = 30$ s, but to predict slightly higher values than typically observed at $\tau = 60$ s. The discrepancy at long times could be explained by technical sources of heating at the 1 nK s^{-1} level or lower.

Naturally, it is important to ensure that the fluctuations observed in figure 24 truly reflect the underlying dynamics of the gas being sampled, rather than other sources of experimental noise. For instance, fluctuations in the trap bias field cause the total number of atoms observed to fluctuate by $\sim 10^4$ from one repetition to the next, which might reasonably impact the observed condensate number. However, if the variations in N_0 were caused by such an effect, the measured values should be correlated with those of the responsible parameter. Contingency-square analysis [73] was used to

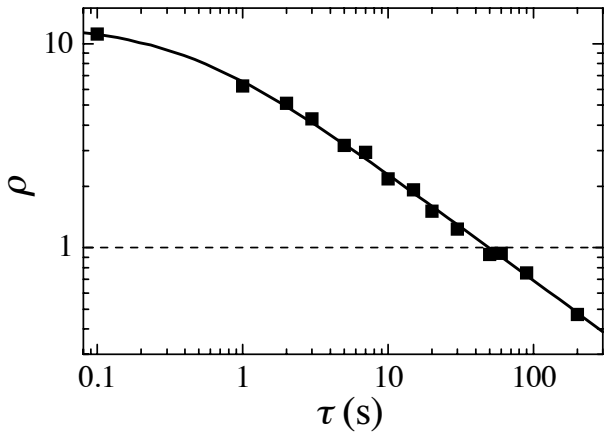

Figure 27. Equilibration of a degenerate gas. The critical parameter ϱ of equation (110) is shown as a function of delay time after the microwave sweep τ.

determine that no statistically significant correlation exists with changes in N, T, phase-space density, loading conditions, evaporative cooling trajectory, probe parameters, goodness of fit or from one measurement to the next. We therefore conclude that the variations are intrinsic to the gas.

4.3. Equilibration

The cycle of condensate growth and collapse is driven by an excess of noncondensed atoms compared to a thermal distribution. This excess can be examined directly. Doing so provides a check on the interpretation of the histogram data, since the changing shape of the distributions should be consistent with the approach to equilibrium. The equilibration process is also interesting in its own right, as it demonstrates significant differences from the behaviour of a nondegenerate gas.

The experimental procedures and analysis are exactly those used to generate the histogram data. However, instead of considering the values of N_0 obtained, the total number N and temperature parameter β are used to calculate

$$\varrho \equiv \frac{N}{N_c} = 0.832\, N(\beta\hbar\omega)^3 \qquad (110)$$

as a function of delay time τ. The results obtained are shown in figure 27. Because of the fluctuations in the trap bias field, ϱ varies by ~40% from one run to the next, and the points shown are averages over several repetitions at each τ. Also, systematic errors in N and β limit the accuracy of ϱ to roughly 30%. This is reduced for $\varrho \leqslant 1$ by fitting the images to an equilibrium Bose–Einstein distribution function, which then gives an uncertainty of approximately 10%.

Because N_m is small compared to N, equilibrium is reached when $\varrho \approx 1$. As can be seen from figure 27, this occurs at $\tau \approx 50$ s on average. Comparison with figure 24 shows that this is consistent with the time at which the shape of the histograms begins to change, helping to confirm the interpretation of the histograms as reflecting the underlying dynamical behaviour.

For each value of τ in figure 27, the microwave sweep at the end of evaporative cooling was adjusted to maintain

the average number N constant at $\sim 2 \times 10^4$ atoms, to agree with the data used for the histogram plots. Because of this, the points shown do not represent the evolution of any single cloud in time, making interpretation slightly more difficult. This approach was used because the trap bias field drifts, and the sweep must be occasionally adjusted to maintain a constant average N.

The solid curve in figure 27 is a fit to a power law form

$$\varrho(\tau) = \varrho_1(1 + \kappa\tau)^{\gamma_\varrho}, \tag{111}$$

with $\varrho_1 = 12.5$, $\kappa = 2.5\ \mathrm{s}^{-1}$ and $\gamma_\varrho = -0.52$. A power-law form is to be expected, since the QBE is nonlinear. Of particular interest is the exponent γ_ϱ, since it should be comparable with theoretical predictions.

For such a comparison to be made, it is necessary to correct for the variation in initial conditions. If the number and temperature also vary according to a power law, as

$$N(t) = N_1(1 + \kappa\tau)^{\gamma_N} \tag{112}$$

and

$$T(t) = T_1(1 + \kappa\tau)^{\gamma_T} \tag{113}$$

respectively, then

$$\varrho(\tau) \sim \frac{N_1}{T_1^3}\,(1 + \kappa\tau)^{\{\gamma_N - 3\gamma_T\}}. \tag{114}$$

In the experiment, both N_1 and T_1 are varied with τ, but the measured values are observed to be related as $T \propto N^{1/2}$. This is the expected relation for a harmonic trap. Therefore, because N is held fixed, N_1 must vary as $\tau^{-\gamma_N}$ and T_1 as $\tau^{-\gamma_N/2}$. Thus,

$$\varrho(\tau) \propto \frac{N}{T_1^3(1 + \kappa\tau)^{3\gamma_T}} \propto (1 + \kappa\tau)^{3\gamma_N/2 - 3\gamma_T}, \tag{115}$$

and the experimental exponent is $\gamma_\varrho = 3(\gamma_N/2 - \gamma_T)$.

The evolution of N and T can be predicted using the QBE simulation, which gives $\gamma_N = -0.2$ and $\gamma_T = 0.1$. The observed γ_ϱ is thus predicted to be -0.6, in reasonable agreement with the experiment. The values of γ_N and γ_T are, however, surprising. For a nondegenerate gas decaying via two-body inelastic collisions, it can be shown that $\gamma_N = -8/11$ and $\gamma_T = 2/11$, considerably different than observed. The exponents obtained in the QBE model are found to be independent of the value of the loss coefficient G_2, and of the trap depth E_T applied after the microwave sweep. The difference therefore appears to be a signature of the nonclassical nature of the Bose–Einstein distribution function.

It is interesting to consider what mechanism is mainly responsible for reducing the excess of atoms and allowing the gas to equilibrate. Two loss mechanisms are included in the model, dipolar relaxation and the collapse. In the trajectory shown in figure 13, 15 collapses occur, in which 1.6×10^4 atoms are ejected from the trap. Between the microwave sweep and the final collapse, a total of 2.4×10^4 atoms are lost, so the collapses and dipolar relaxation both play important roles. The rise in temperature during equilibration is also important, but the effects of the collapse and of dipolar decay are more difficult to distinguish. Estimating the average energy gained through the two processes, however, again suggests that both contribute at a similar level.

5. Conclusions and new results

The work described here offers two main results regarding the behaviour of Bose gases with negative scattering length. The first is the theoretical predictions obtained by modelling the QBE. For nondegenerate gases, this has provided information on evaporative cooling to support the experiments. For degenerate gases, a cycle of condensate growth and collapse is observed. Although this behaviour can be qualitatively understood in terms of simpler models, the full calculation of the QBE is useful, as it gives detailed and quantitative predictions which can be meaningfully compared to experiment. Of particular interest are the frequency of the oscillations, the time for which they continue and the characteristic shape of condensate growth after a collapse.

Several questions remain to be answered, however. There is as yet no good theoretical model of the collapse process itself, which limits the accuracy of the QBE results. First, an accurate prediction for the state of the condensate after a collapse is needed, with both the number of atoms remaining and their excitation energy being important. In addition, the effect of excitations on the subsequent dynamics of the condensate must be better understood. This can likely be accomplished through further analysis of the NLSE, although the correct way to account for losses from inelastic collisions is not yet clear.

A more difficult question is how to treat the interaction between the condensate and the noncondensed cloud. This interaction works two ways: the addition of atoms to the condensate as the gas cools will both depend on and affect the state of the condensate. Modelling this situation requires the inclusion of both coherent and incoherent dynamics, so neither the NLSE nor the QBE will suffice by themselves. Stoof has formulated a scheme in which these effects are combined in a single Fokker–Plank equation governing the condensate [61], but a full and realistic solution to the problem remains challenging.

On the experimental side, the central result of this work is the measurement of the distribution of N_0 values described in section 4. This result provides strong, if indirect, evidence that the theoretical predictions for the condensate dynamics are at least qualitatively correct. Furthermore, the detailed shape of the distributions allows quantitative comparison with theory. The data suggest that on the order of $N_m/6$ atoms remain in the condensate after a collapse, but that this number fluctuates considerably. No currently available theory is able to reproduce this result.

Since the work described here was completed, however, two new experiments have been performed which corroborate and extend the results obtained. First is the achievement of BEC in a gas of ^{85}Rb atoms [15]. The unperturbed scattering length in this case is approximately -20 nm, so large that N_0 is limited to about 80 atoms. However, in a magnetic field of 155 G, ^{85}Rb atoms undergo a so-called Feshbach resonance, near which the scattering length depends strongly on the magnetic field strength. By exploiting this sensitivity, the researchers were able to achieve BEC in a regime with positive a, and then change a to be negative. Upon doing so, they observe that a collapse does indeed occur, as predicted. In these experiments, a small number of atoms remained in the condensate after the collapse, in qualitative agreement with

the result presented here. Direct comparison of the results is complicated by the fact that the ^{85}Rb experiments took place at much lower temperatures, and in a trap with significantly different asymmetry. In addition, the collapse was initiated with N_0 far in excess of N_m, and consequently with high initial energy. In this case, the collapse mechanisms of quantum tunnelling and thermal excitation are not relevant.

A second new experiment was carried out using ^{7}Li, in the apparatus described above [74]. Here a photoassociation technique was used to selectively remove the condensate population of a degenerate gas. Because of the presence of the thermal gas, the condensate subsequently refilled, and this filling could be observed directly. Furthermore, when N_0 approached its maximum value, a sudden decrease occurred, exactly as predicted by the collapse/fill model. These two experiments demonstrate direct agreement with our understanding of BEC in a gas with attractive interactions, and also point the way to more explicit and quantitative comparisons with theory.

Acknowledgments

We are grateful to acknowledge the contributions of C Bradley, J Gerton, H Stoof, J Tollett and M Welling to the work reported here. This work was supported by the National Science Foundation and the Welch Foundation.

References

[1] Einstein A 1925 *Sitzungsber. Preuss. Akad. Wissen., Physik.-Mathem. Klasse* 3
[2] Bose S N 1924 *Z. Phys.* **26** 178
[3] London F 1938 *Nature* **141** 643
[4] Tisza L 1938 *Nature* **141** 913
[5] Bardeen J, Cooper L N and Schrieffer J R 1957 *Phys. Rev.* **106** 162
[6] Snoke D W, Wolfe J P and Mysyrowicz A 1990 *Phys. Rev. Lett.* **64** 2543
[7] Lin J L and Wolfe J P 1993 *Phys. Rev. Lett.* **71** 1222
[8] Crooker B C, Hebral B, Smith E N, Takano Y and Reppy J D 1983 *Phys. Rev. Lett.* **51** 666
[9] Chan M, Mulders N and Reppy J 1996 *Phys. Today* **49** 30
[10] Safonov A I, Vasilyev S A, Yasnikov I S, Lukashevich I I and Jaakkola S 1998 *Phys. Rev. Lett.* **81** 4545
[11] Anderson M H, Ensher J R, Matthews M R, Wieman C E and Cornell E A 1995 *Science* **269** 198
[12] Bradley C C, Sackett C A, Tollett J J and Hulet R G 1995 *Phys. Rev. Lett.* **75** 1687
[13] Davis K B, Mewes M O, Andrews M R, van Druten N J, Durfee D S, Kurn D M and Ketterle W 1995 *Phys. Rev. Lett.* **75** 3969
[14] Fried D G, Killian T C, Willmann L, Landhuis D, Moss S C, Kleppner D and Greytak T J 1998 *Phys. Rev. Lett.* **81** 3811
[15] Cornish S L, Claussen N R, Roberts J L, Cornell E A and Wieman C E 2000 *Phys. Rev. Lett.* **85** 1795
[16] Jin D S, Ensher J R, Matthews M R, Wieman C E and Cornell E A 1996 *Phys. Rev. Lett.* **77** 420
[17] Mewes M O, Andrews M R, van Druten N J, Kurn D M, Durfee D S, Townsend C G and Ketterle W 1996 *Phys. Rev. Lett.* **77** 988
[18] Burt E A, Ghrist R W, Myatt C J, Holland M J, Cornell E A and Wieman C E 1997 *Phys. Rev. Lett.* **79** 337
[19] Ketterle W and Miesner H J 1997 *Phys. Rev.* A **56** 3291
[20] Andrews M R, Townsend C G, Miesner H J, Durfee D S, Kurn D M and Ketterle W 1997 *Science* **275** 637
[21] Hall D S, Matthews M R, Wieman C E and Cornell E A 1998 *Phys. Rev. Lett.* **81** 1543
[22] Myatt C J, Burt E A, Ghrist R W, Cornell E A and Wieman C E 1997 *Phys. Rev. Lett.* **78** 586
[23] Stamper-Kurn D M, Andrews M R, Chikkatur A P, Inouye S, Miesner H J, Stenger J and Ketterle W 1998 *Phys. Rev. Lett.* **80** 2027
[24] Huang K 1987 *Statistical Mechanics* 2nd edn (New York: Wiley)
[25] Kittel C and Kroemer H 1980 *Thermal Physics* 2nd edn (New York: Freeman)
[26] Ashcroft N W and Mermin N D 1976 *Solid State Physics* (Philadelphia, PA: Saunders)
[27] Meystre P and Sargent M 1991 *Elements of Quantum Optics* 2nd edn (Berlin: Springer)
[28] Andrews M R, Mewes M O, van Druten N J, Durfee D S, Kurn D M and Ketterle W 1996 *Science* **273** 84
[29] Abraham E R I, McAlexander W I, Gerton J M, Hulet R G, Côté R and Dalgarno A 1997 *Phys. Rev.* A **55** R3299
[30] Landau L D and Lifshitz E M 1958 *Statistical Physics* 1st edn (London: Pergamon)
[31] Stoof H T C 1994 *Phys. Rev.* A **49** 3824
[32] Ruprecht P A, Holland M J, Burnett K and Edwards M 1995 *Phys. Rev.* A **51** 4704
[33] Hall D S, Matthews M R, Ensher J R, Wieman C E and Cornell E A 1998 *Phys. Rev. Lett.* **81** 1539
[34] Joachain C J 1975 *Quantum Collision Theory* 3rd edn (Amsterdam: Elsevier)
[35] Townsend J S 1992 *A Modern Approach to Quantum Mechanics* (New York: McGraw-Hill)
[36] Fetter A L and Walecka J D 1971 *Quantum Theory of Many-Particle Systems* (New York: McGraw-Hill)
[37] Lifshitz E M and Pitaevskii L P 1980 *Statistical Physics* Part II (Oxford: Butterworth–Heineman)
[38] Dalfovo F, Giorgini S, Pitaevskii L P and Stringari S 1999 *Rev. Mod. Phys.* **71** 463
[39] Houbiers M and Stoof H T C 1996 *Phys. Rev.* A **54** 5055
[40] Bergeman T 1997 *Phys. Rev.* A **55** 3658
[41] Baym G and Pethick C J 1996 *Phys. Rev. Lett.* **76** 6
[42] Shuryak E V 1996 *Phys. Rev.* A **54** 3151
[43] Stoof H T C 1997 *J. Stat. Phys.* **87** 1353
[44] Singh K G and Rokhsar D S 1996 *Phys. Rev. Lett.* **77** 1667
[45] Kagan Yu, Shlyapnikov G V and Walraven J T M 1996 *Phys. Rev. Lett.* **76** 2670
[46] Ueda M and Leggett A J 1998 *Phys. Rev. Lett.* **80** 1576
[47] Yuen H C and Ferguson J W E 1978 *Phys. Fluids* **21** 1275
[48] Zhakharov V E 1972 *Sov. Phys.–JETP* **35** 908
[49] Zhakharov V E and Synakh V S 1975 *Sov. Phys.–JETP* **41** 465
[50] Dyachenko S, Newell A C, Pushkarev A and Zakharov V E 1992 *Physica* D **57** 96
[51] Kagan Yu, Muryshev A E and Shlyapnikov G V 1998 *Phys. Rev. Lett.* **81** 933
[52] Sackett C A, Bradley C C and Hulet R G 1997 *Phys. Rev.* A **55** 3797
[53] Sackett C A, Stoof H T C and Hulet R G 1998 *Phys. Rev. Lett.* **80** 2031
[54] Hillery M, O'Connell R F, Scully M O and Wigner W P 1984 *Phys. Rep.* **106** 102
[55] Akhiezer A I and Peleminskii S V 1981 *Methods of Statistical Physics* (New York: Pergamon)
[56] Luiten O J, Reynolds M W and Walraven J T M 1996 *Phys. Rev.* A **53** 381
[57] Surkov E L, Walraven J T M and Shlyapnikov G V 1996 *Phys. Rev.* A **53** 3403
[58] Wu H and Foot C J 1996 *J. Phys. B: At. Mol. Opt. Phys.* **29** 321
[59] Holland M, Williams J, Coakley K and Cooper J 1996 *Quantum Semiclass. Opt.* **8** 571
[60] Gardiner C W, Zoller P, Ballagh R J and Davis M J 1997 *Phys. Rev. Lett.* **79** 1793
[61] Stoof H T C 1999 *J. Low Temp. Phys.* **114** 11
[62] Wu H, Arimondo E and Foot C J 1997 *Phys. Rev.* A **56** 560
[63] Holland M, Williams J and Cooper J 1997 *Phys. Rev.* A **55** 3670
[64] Ketterle W and van Druten N J 1996 *Advances in Atomic,*

Molecular, and Optical Physics vol 37, ed B Bederson and H Walther (San Diego: Academic) p 181
[65] Gerton J M, Sackett C A, Frew B J and Hulet R G 1999 *Phys. Rev.* A **59** 1514
[66] Bradley C C, Sackett C A and Hulet R G 1997 *Phys. Rev. Lett.* **78** 985
[67] Tollett J J, Bradley C C, Sackett C A and Hulet R G 1995 *Phys. Rev.* A **51** R22
[68] Sackett C A, Bradley C C, Welling M and Hulet R G 1997 *Appl. Phys.* B **65** 433
[69] Bradley C C and Hulet R G 1996 *Atomic, Molecular, and Optical Physics: Atoms and Molecules* ed F B Dunning and R G Hulet (San Diego: Academic) p 129
[70] Born M and Wolf E 1980 *Principles of Optics* 6th edn (Oxford: Pergamon)
[71] Hecht E 1987 *Optics* 2nd edn (Reading, MA: Addison-Wesley)
[72] Bradley C C, Sackett C A and Hulet R G 1997 *Phys. Rev.* A **55** 3951
[73] Press W H, Teukolsky S A, Vetterling W T and Flannery B P 1992 *Numerical Recipes in C: The Art of Scientific Computing* 2nd edn (Cambridge: Cambridge University Press)
[74] Gerton J M, Strekalov D, Prodan I and Hulet R G 2000 *Nature* **408** 692